Modeling the contribution of leads to sea spray aerosol in the high Arctic

Rémy Lapere, Louis Marelle, Pierre Rampal, Laurent Brodeau, Christian Melsheimer, Gunnar Spreen, Jennie L Thomas

Atmos. Chem. Phys., 24, 12107–12132, 2024
https://doi.org/10.5194/acp-24-12107-2024

Atmospheric Chemistry and Physics
Open Access
EGU

Modeling the contribution of leads to sea spray aerosol in the high Arctic

Rémy Lapere[1,2], Louis Marelle[2], Pierre Rampal[1], Laurent Brodeau[1,4], Christian Melsheimer[3], Gunnar Spreen[3], and Jennie L. Thomas[1]

[1]Univ. Grenoble Alpes, CNRS, INRAE, IRD, Grenoble INP, IGE, 38000 Grenoble, France
[2]LATMOS/IPSL, Sorbonne Université, UVSQ, CNRS, 75005 Paris, France
[3]Institute of Environmental Physics (IUP), University of Bremen, Bremen, Germany
[4]DATLAS, 38000 Grenoble, France

Correspondence: Rémy Lapere (remy.lapere@latmos.ipsl.fr) and Jennie L. Thomas (jennie.thomas@univ-grenoble-alpes.fr)

Received: 29 April 2024 – Discussion started: 6 May 2024
Revised: 9 September 2024 – Accepted: 12 September 2024 – Published: 30 October 2024

Abstract. Elongated open-water areas in sea ice (leads) release sea spray particles to the atmosphere. However, there is limited knowledge on the amount, properties and drivers of sea spray emitted from leads, and no existing parameterization of this process is available for use in models. In this work, we use measurements of aerosol fluxes from Nilsson et al. (2001) to produce an estimate of the location, timing and amount of sea spray emissions from leads at the scale of the Arctic Ocean for 1 year. Lead fractions are derived using sea ice data sets from numerical models and satellite detection. The proposed parameterization estimates that leads account for 0.3 %–9.8 % of the annual sea salt aerosol number emissions in the Arctic Ocean regions where sea ice concentration is greater than 80 %. Assuming similar size distributions to those from emissions from the open ocean, leads account for 30 %–85 % of mass emissions in sea ice regions. The total annual mass of sea salt emitted from leads, 0.1–2.1 Tg yr^{-1}, is comparable to the mass of sea salt aerosol transported above sea ice from the open ocean, according to the MERRA-2 reanalysis. In addition to providing the first estimates of possible upper and lower bounds of sea spray emissions from leads, the conceptual model developed in this work is implemented and tested in the regional atmospheric chemistry model WRF-Chem. Given the estimates obtained in this work, the impact of sea spray from leads on Arctic clouds and radiative budget needs to be further explored.

1 Introduction

Aerosols resulting from sea spray make up most of the aerosol mass over the polar regions (Sand et al., 2017) and are a critical driver of polar climate (Struthers et al., 2011; Lapere et al., 2023). Sea spray is the mix of sea salt and organics co-emitted together from oceanic sources. These aerosols impact clouds, precipitation and climate, as they can act as cloud condensation nuclei (CCN) or ice-nucleating particles (INPs) depending on their composition (i.e., fraction of inorganic salts and organic matter) and processing in the atmosphere (Quinn et al., 2017; Fossum et al., 2018; Wilson et al., 2015; DeMott et al., 2016). Sea spray particles also contribute to the aerosol direct radiative effect by scattering incoming solar shortwave radiation (Takemura et al., 2002; Satheesh and Lubin, 2003). In addition, sea spray aerosols can change the climate impact of aerosols of other origins through mixing, such as nitrate (Chen et al., 2020) and sulfate (Fossum et al., 2020), by regulating their droplet activation. Similarly, changes in sea spray aerosols can impact the condensation sink in the Arctic, which in turn affects new particle formation and therefore the CCN populations (Browse et al., 2014), although results vary for different models (Gilgen et al., 2018).

Sea spray emissions in the mid-latitude oceans are driven by wind action that generates whitecaps, which release

aerosols into the atmosphere through seawater bubble bursting (Monahan et al., 1986). In the high Arctic, where the ocean can be partially or fully covered by sea ice, additional polar-specific sources of sea salt emissions include blowing snow over sea ice (Yang et al., 2008; Huang and Jaeglé, 2017; Yang et al., 2019; Marelle et al., 2021; Frey et al., 2020) and sea spray from leads (Nilsson et al., 2001; Leck et al., 2002; Held et al., 2011; Kirpes et al., 2019). Studies have suggested frost flowers as another potential sea ice source of sea salt aerosol in Arctic coastal regions (Domine et al., 2004; Xu et al., 2016), although the extent to which they contribute is still uncertain (Huang et al., 2018; Kirpes et al., 2019). Sea salt aerosols generated through sublimation of saline blowing snow have been included in several atmospheric models (Yang et al., 2008, 2019; Huang and Jaeglé, 2017; Marelle et al., 2021; Gong et al., 2023). However, a dedicated parameterization for sea spray emissions from leads is not available. Leads are fractures in sea ice wide enough to be navigable by vessels (WMO, 2014). They typically have an elongated shape, with lengths from hundreds of meters to hundreds of kilometers and widths from tens of meters to kilometers (Li et al., 2020). Sea spray in regions of leads are usually modeled identically to open-ocean emissions, weighted by the open-water fraction within the grid cell (e.g., Ioannidis et al., 2023), although it is known that leads have properties that make the emission process different from the open ocean (e.g., Nilsson et al., 2001). The measured emissions over leads and the open ocean show that there are (1) differences in the magnitude of sea spray particle emissions (number and mass), suggesting different driving mechanisms (Nilsson et al., 2001; May et al., 2016), and (2) differences in the composition of sea spray, with enhanced organic fraction when coming from leads (Leck et al., 2002; Kirpes et al., 2019). Therefore, models with a detailed representation of sea spray emissions from leads are needed to accurately represent their contribution to aerosol–radiation and aerosol–cloud interactions (Thornhill et al., 2021). In particular, in the warming Arctic as sea ice extent and thickness changes and the marginal ice zone (MIZ) becomes wider at certain times of year (Strong and Rigor, 2013), emissions from leads may be relatively more or less important than emissions from the open ocean or pack ice. Not including this process in models may lead to an incomplete knowledge of the changing natural aerosol baseline in the Arctic, which may affect our representation of the Arctic climate.

There have been a limited number of dedicated measurements to quantify sea spray emissions from leads. Radke et al. (1976) measured sodium (Na^+) aerosol and CCN atmospheric concentrations at Utqiaġvik, Alaska, in March 1970 and found a correlation between lead openings near the station and increased Na^+ concentrations but that lead occurrence had limited impact on CCN concentrations. Nilsson et al. (2001) measured aerosol turbulent fluxes over leads in the high Arctic in July–August 1996. They found (i) that emissions are larger over the open ocean than over leads by about an order of magnitude and (ii) that the size distribution of aerosols is dominated by a 2 µm diameter mode over leads, while there are two modes (100 nm and 1 µm) for open-ocean emissions. Processes related to biological activity, the release of supersaturated gases, or sea ice melt were suggested to explain the formation and bursting of bubbles releasing sea spray in leads rather than whitecaps like over the open ocean. They also concluded that sea spray emissions from leads may be important for CCN populations in the Arctic. Leck et al. (2002) also suggested a non-wind-driven bubble-bursting process, mostly active during sea ice melting days, consisting mainly of small-bubble-sourced jet drop mode emissions. This study also showed fractions of organics in sea spray from leads of up to 20 % (in volume) in the high Arctic in July–August 1996. They also suggested that the increased organic fraction of sea spray reduced their CCN activity. Held et al. (2011) suggested that emissions from leads could explain 5 %–10 % of the variations in measured particle number concentrations in August 2008 in the high Arctic. They also showed that elevated aerosol concentrations were more frequently observed over leads than over the continuous pack ice. May et al. (2016) showed that, over the period 2006–2009, the super-micrometer Na^+ aerosol mass can be multiplied by 4 when leads open near Utqiaġvik, Alaska, while sub-micrometer aerosols are more affected by long-range transport. This conclusion is based on a measured shift in mass distribution towards larger aerosol sizes when leads are present and a greater influence of transported sea salt aerosol in a more continuous sea ice cover condition. Kirpes et al. (2019) demonstrated the need for inclusion of lead-sourced sea spray production in the modeling of Arctic atmospheric composition and quantified the median organic fraction in emissions from leads between 30 % to 50 % at Utqiaġvik, Alaska, for 6 winter days in 2014. They further indicate that the observed organic coating could come from cryoprotectant gels produced by micro-organisms. At the same site and in spring 2016, Chen et al. (2022) also showed the important role played by leads both in sea salt aerosol direct emission and through deposition of sea spray onto snow, which has the potential to be re-suspended later through blowing snow, although their measurements could not make a conclusion on this last part.

In summary, sea spray emissions (mass and number) from leads (i) are probably comparable in magnitude but lower than emissions from the open ocean; (ii) might have higher organic contents than over open oceans; and (iii) have a different size distribution than open-ocean sea spray, with a dominant coarse mode. However, not enough information exists for both points (ii) and (iii) in order for these conclusions to be transferred directly for use in atmospheric emissions within models. Therefore, the parameterization proposed within this paper focuses on point (i) with the aim of exploring the possible range of sea spray emissions from leads at the scale of the Arctic. We also evaluate how this compares to the blowing-snow source of sea salt aerosols

and long-range transport of sea salt from lower latitudes to the high Arctic, in order to motivate future work refining the approach to account for points (ii) and (iii). In order to better understand the role of leads in the Arctic aerosol budget, this paper addresses the following scientific questions.

- How can atmospheric models estimate sea spray emissions from leads from the current state of knowledge?
- What are the likely upper and lower bounds of sea spray emissions from leads in the Arctic?
- What is the modeled annual cycle of sea spray emissions from leads and how does it compare with blowing snow?
- What is the sensitivity of Arctic sea salt aerosol to sea spray emissions from leads?

To address these questions we first present a conceptual model of sea spray emissions from leads and the main methodological assumptions to formulate them for the Arctic Ocean in Sect. 2. Section 3 presents the sea spray emissions obtained from the conceptual model for the year 2018 and the sensitivity of these emissions to input parameters and compares the modeled sea spray emissions from leads with other sources of sea salt aerosol over the high Arctic Ocean (blowing snow and transport). The impact of this parameterization on atmospheric concentrations of sea salt is further evaluated using the Weather Research and Forecasting model coupled with Chemistry (WRF-Chem). The implications of this work are finally discussed in Sect. 4.

2 Materials and methods

2.1 Methods

In this section we present the approach used for the parameterization of sea spray emissions from leads, including the measurements it is based on, the method to compute the inorganic and organic fractions of sea spray, and the parameterization of sea salt emissions from blowing snow for comparison with leads. The conceptual emission model built in this work is implemented in a series of Python3 Jupyter notebooks, available at Lapere (2024). In this work, the conceptual model is used to compute emissions for the year 2018.

2.1.1 Lead flux parameterization

To our knowledge, the only detailed measurements of sea spray aerosol fluxes over leads that can readily be used for modeling purposes are found in Nilsson et al. (2001). They found that the total particle number aerosol flux over the open Norwegian Sea and Barents Sea was described by F_{oo} (in $10^6\,m^{-2}\,s^{-1}$) in Eq. (1), whereas over leads it corresponded to F_{leads} (in $10^6\,m^{-2}\,s^{-1}$). In both cases, the 10 m wind speed (U in $m\,s^{-1}$) appeared as the controlling factor. Unfortunately, the aerosol fluxes reported in Nilsson et al. (2001) are not size-resolved data and cannot be used as is in atmospheric aerosol models. Therefore, we propose to parameterize sea spray emissions from leads by applying a correction factor ($R_{Nilsson}$) to open-ocean sea spray source functions based on commonly used size-resolved sea spray source functions (described below). $R_{Nilsson}$ is calculated as the ratio between aerosol fluxes from the open ocean and leads derived from Nilsson et al. (2001), which depends on 10 m wind speed (Eq. 1 and Fig. 1a).

$$R_{Nilsson} = \frac{F_{leads}}{F_{oo}} = \frac{e^{0.11[\pm0.05]U-1.93}}{e^{0.20[\pm0.06]U-1.71}} \quad (1)$$

The three sea spray source functions used in this work are Gong (2003) (GO03), Salter et al. (2015) (SA15), and Ioannidis et al. (2023) (IO23). GO03, together with Monahan et al. (1986), of which it is an adaptation, is the most commonly used open-ocean sea spray source function in global climate models, such as the ones involved in CMIP6 (Lapere et al., 2023). On the other hand, SA15 departs from the usual whitecap approach and includes a dependency on sea surface temperature (SST), which can be an important factor for polar oceans and leads. Furthermore, the SA15 source function has been tested and validated against measurements at high-latitude stations. Finally, the IO23 source function, implemented in the WRF-Chem model for Arctic studies, also includes a dependency on SST but is based on a whitecap fraction approach, with a correction for smaller aerosols (see Sect. 3.7.1). By using these three functions (the formulations of which are described in Sect. A1), we can compare an approach commonly used in global models (Lapere et al., 2023) with more Arctic-adapted approaches, including a non-whitecap-based approach. The interested reader is invited to use the code of the conceptual model provided with this study to test any other source function. We choose an aerosol diameter cutoff between 10 nm and 10 µm, typical of what most climate and atmospheric chemistry models use for the representation of sea salt aerosols. The size distribution of particles emitted from leads derived from applying $R_{Nilsson}$ to all three source functions is presented in Fig. 1b. These source functions show different magnitudes for small-sized aerosols but similar magnitudes for larger particles.

Because emission fluxes from leads are uncertain, we also use the confidence intervals of the fitting parameters given by Nilsson et al. (2001) to derive the upper and lower possible boundaries for sea spray emissions from leads. The minimum and maximum $R_{Nilsson}$ ratios based on these confidence intervals are described in Eq. (2) and (3), respectively:

$$R_{Nilsson_{min}} = \frac{e^{0.06U-1.93}}{e^{0.26U-1.71}}, \quad (2)$$

and

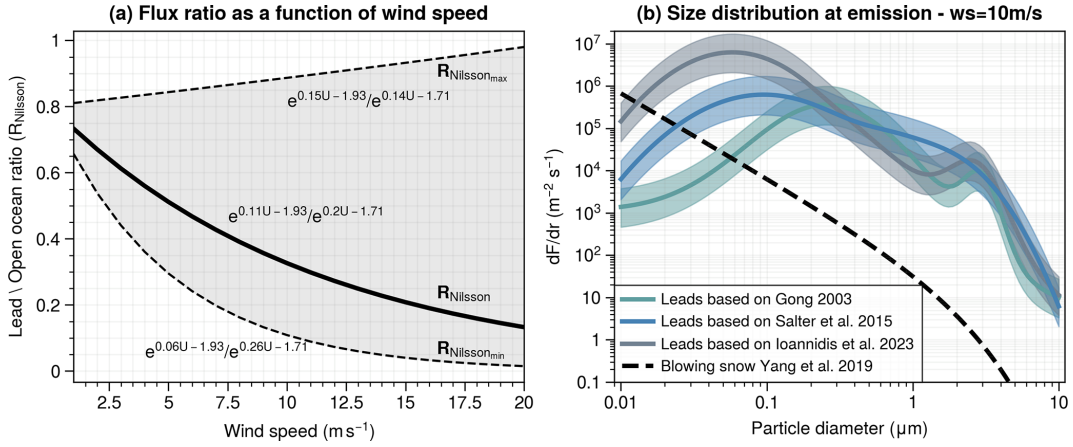

Figure 1. Emission flux parameterization. **(a)** Flux ratio derived from Nilsson et al. (2001) as a function of wind speed. The solid line shows the best-fit coefficients from Nilsson et al. (2001), while the upper and lower dashed lines use the minimum and maximum fit coefficients, respectively. **(b)** Size distribution of sea salt aerosol emissions from leads based on GO03 (green), SA15 for a 2 °C SST (blue) and IO23 for a 2 °C SST (gray), and blowing snow based on Yang et al. (2019) (dashed line) for a salinity of 0.1 psu, relative humidity with respect to ice of 95 %, air temperature of −5 °C and snow age of 3 d, as implemented in this study. Shading indicates data using the minimum and maximum R_{Nilsson} coefficients.

$$R_{\mathrm{Nilsson_{max}}} = \frac{e^{0.15U-1.93}}{e^{0.14U-1.71}}. \quad (3)$$

Figure 1a shows that $R_{\mathrm{Nilsson_{max}}}$ is greater than 0.8 for any wind speed, i.e., lead fluxes are similar to open-ocean fluxes using this ratio, and this increases with wind speed. In contrast, $R_{\mathrm{Nilsson_{min}}}$ is less than 0.3 for wind speeds above 5 m s^{-1} and declines with increasing wind speed, similar to R_{Nilsson}.

2.1.2 Estimating the organic fraction of marine aerosols

Sea spray is generally composed of important fractions of organic material. Here, the organic fraction (OF) of sea spray emissions is computed based on work by Vignati et al. (2010), where the OF (in %) depends only on the chlorophyll *a* surface concentration in the ocean (Chl in µg m^{-3}), as expressed in Eq. (4):

$$\mathrm{OF} = 43.5\,\mathrm{Chl} + 13.805, \quad (4)$$

with limit values of 2 % and 76 %.

For Chl, we use the daily average mass concentration of chlorophyll *a* in seawater from the Global Ocean Biogeochemistry Hindcast provided by the Copernicus Marine Service Information (Copernicus Marine Service Information, 2023b). Although products such as Copernicus Marine Service Information (2023b) cannot be validated in leads due to the lack of sufficient amount of in situ data and model biases in under-ice phytoplankton phenology and sea ice coverage (Wakamatsu et al., 2022), this is the best available option for our purpose. We tested several parameterizations for sea spray OF that connect chlorophyll *a* to OF with a simple relationship, including Vignati et al. (2010), Rinaldi et al. (2013), and Gantt et al. (2015) (results not shown here). We found that Vignati et al. (2010) yielded the most realistic values for the Arctic compared to measurements from Leck et al. (2002) and Kirpes et al. (2019) (see Sect. 3.5). For consistency, the OF parameterization is used both in the conceptual model (Sect. 3.1 through 3.5) and in WRF-Chem (Sect. 3.7) to estimate the marine organic aerosol emissions. As noted in the Sect. 1, sea spray refers to the full emission flux (sea salt and OF). Sea salt is defined as the sea spray flux minus its organic fraction (sea_spray · [1 − OF]). The uncertainty in the Copernicus Marine Service Information (2023b) product will therefore only affect the partitioning between inorganic sea salt and marine organics and not the total sea spray emission flux. In this work, the size distribution of organics is assumed to be the same as inorganic sea salt, which is a first estimate. Future work that refines the size distribution of marine organic emissions from leads is needed, as measurements have shown that inorganic sea salt and marine organics have different dominant modes (Prather et al., 2013; Wang et al., 2017), including in the Arctic (Kirpes et al., 2019).

We acknowledge that there are limitations associated with parameterizing organic fraction using chlorophyll *a*. However, the availability of chlorophyll *a* products makes it more likely that these parameterizations can be adapted and used within climate and Earth system models. While it is clear that other seawater characteristics than chlorophyll *a* (such as organic carbon or glucose concentration) can better account for the OF of sea spray (Fuentes et al., 2010; Quinn et al., 2014; Rocchi et al., 2024), their lack of general availabil-

ity in satellite- or model-based products limits our ability to recommend these now for use by large-scale models.

2.1.3 Estimating sea salt aerosol from blowing snow

In addition to leads, blowing snow is an important source of sea salt aerosol in the Arctic, but the relative importance of blowing snow and leads for the Arctic sea salt aerosol budget is still an open question. In order to compare the emissions from leads obtained with our parameterization with sea salt emissions from blowing snow, we use the existing blowing-snow emission parameterization described in Yang et al. (2008, 2019). The size-resolved fluxes from leads and blowing snow are compared in Fig. 1b.

Although this blowing-snow parameterization bears uncertainties, including snow salinity, number of sea salt aerosols released per snow grain and fitting parameters (threshold wind speeds, surface temperatures, effect of snow age…), this work does not aim to investigate these uncertainties. The tuning parameters used here correspond to the ones used in Gong et al. (2023) and Confer et al. (2023), where more extensive validations against Arctic observations were conducted. In particular, Confer et al. (2023) showed that using variable or fixed snow salinity can change the total emission flux by 72 %. As a result, the blowing-snow fluxes are given as indicative for comparison with leads but are not representative of the range of possible actual values, which are still uncertain and would require more observations to be estimated.

To evaluate where and when blowing-snow events can occur, i.e., where there is enough fresh snow that can be mobilized, we consider the surface snow thickness from the daily Arctic Ocean Physics Reanalysis (Copernicus Marine Service Information, 2023a). If snow thickness on sea ice decreases from one day to the other, we consider there to have been melt or strong snow drift and deem that the snow can no longer be mobilized. Blowing snow is considered to be able to occur otherwise. Although this assumption is a simplification, it is more realistic than the current state of modeling of blowing snow in atmospheric models, which usually assumes an infinite snow reservoir on sea ice. The difference between these two approaches (blowing-snow source limited by decreased snow on sea ice cover versus snow on sea ice always available for lofting) is tested in Sect. 3.6.

2.2 Sea ice data, lead detection and meteorological data

2.2.1 Lead fraction derived from TOPAZ reanalysis

Sea ice concentration information in climate models and atmospheric chemistry models often relies on ocean reanalysis products such as the coupled ocean–sea ice Hybrid Coordinate Ocean Model (CICE) Tracers of Phytoplankton with Allometric Zooplankton (TOPAZ) (Sakov et al., 2012; Copernicus Marine Service Information, 2023a). This data set provides daily Arctic sea ice area fraction, with a 12.5 km spatial resolution. Using this product, we assume that the lead fraction within a given grid cell is the fraction of open ocean, i.e., (1 − sea_ice_concentration), whenever the sea ice concentration is above 80 %. Below this threshold we consider there to be no leads. This value is chosen because it corresponds to the value that is sometimes used to define the transition between the MIZ and the pack ice (e.g., Vichi, 2022). The sensitivity to the selected threshold value is discussed in Appendix A. We note that this concept estimates the fraction of open-water leads, which are the ones relevant for sea salt aerosol fluxes. In other contexts leads may be also covered by thin ice.

2.2.2 Lead fraction derived from NEMO-neXtSIM model

In addition to TOPAZ, we also use the sea ice concentration simulated by the coupled ocean–sea ice Nucleus for European Modelling of the Ocean – Next Generation Sea Ice Model (NEMO-neXtSIM) modeling system (Rampal et al., 2016; Boutin et al., 2023, 2024). NEMO-neXtSIM differs from TOPAZ in various aspects. In particular, this model includes a brittle rheology (the Bingham Maxwell rheology of Ólason et al., 2022) to simulate the sea ice mechanical response to winds and ocean currents. It was shown to be capable of simulating very similar sea ice deformation statistics and scaling properties compared to what is found in satellite observations (Rampal et al., 2019; Ólason et al., 2022), particularly regarding those driving the formation of leads (Ólason et al., 2021).

This sea ice concentration data set is hereafter referred to as neXtSIM (Boutin et al., 2024). The outputs originally consisted of 6-hourly fields that were given on a regular grid of 12 km horizontal spatial resolution for the high Arctic region. However, we work with the daily averaged fields computed from these original files. We define leads in this simulation the same way as in the TOPAZ model, i.e., as the fraction of open ocean where sea ice concentration is larger than 80 %.

2.2.3 Lead fraction from satellite detection

Satellite-derived lead detection products are also available, such as in Willmes et al. (2023a), who provide pan-Arctic daily maps of lead detection based on thermal contrast from the Moderate Resolution Imaging Spectroradiometer (MODIS) data. This product is hereafter referred to as ArcLeads. The spatial resolution of ArcLeads is 1 km, and the time period covered is November to April for the years 2002 to 2021. In their product, Willmes et al. (2023a) classify data in grid cells according to six categories (cloud, land, sea ice, artifact, lead and open water). These data are only available for cloud-free cases; therefore, there can be gaps in the daily data set. Leads in this data set are also not necessarily free of ice. According to the sea ice nomenclature defined by WMO, leads can have ice up to 30 cm thickness (WMO, 2014). The

exact upper ice thickness limit for the ArcLeads product is not known. As ice-covered leads will not allow sea spray aerosol fluxes, these aspects need to be considered in the interpretation.

2.2.4 Spatial processing of sea ice data

The lead fraction we consider from models is not strictly a lead fraction as it includes all areas of open water within the pack ice where the sea ice concentration is greater than 80 %. In coastal regions and the MIZ, it is challenging to differentiate leads from other open-water areas, such as polynyas (Ólason et al., 2021). In order to avoid falsely computing emissions from leads in these regions, a mask excluding coastal regions and MIZ is created and applied on all surface products to ensure we only consider regions where the confidence in lead modeling and detection is higher (black contour in Fig. 2). The area inside this contour is referred to as the high Arctic. We acknowledge that there are also actual leads outside the contour depending on season, especially in the marginal seas. For a conceptual understanding of sea spray aerosol emissions from leads, however, we chose to focus only on the high-confidence area for lead detection and modeling.

Furthermore, all data sets are regridded onto the TOPAZ grid, which is the grid with the lowest resolution. For the ArcLeads satellite product, the number of 1 km grid cells that are flagged as a lead within each 12.5 km TOPAZ grid cell are divided by the total number of ArcLeads cells within the cell. This computation yields the ArcLeads lead fraction inside each TOPAZ grid cell. Leads are relatively small-scale structures, with a typical width from 50 m up to several kilometers (Li et al., 2020), meaning the resolution of 12.5 km used here is not ideal for reproducing individual leads. However, the objective of this work is not to investigate the behavior of individual leads but to estimate emissions from leads at the Arctic scale. In addition, the target application of the emission model provided in this work is regional- to large-scale models, which are seldom run below resolutions of 10 km for polar studies. Therefore, the 12.5 km TOPAZ resolution is appropriate for both the purposes of this work and its foreseen applications.

2.2.5 Meteorological data

In order to calculate the sea spray and blowing-snow emissions, meteorological data are needed. In the conceptual model, we use the 10 m wind speed and 2 m air temperature from the ECMWF Reanalysis v5 (ERA5) hourly reanalysis (Copernicus Climate Change Service, 2017), which we resample to a daily frequency. Additional data sets used in this work also include the Modern-Era Retrospective analysis for Research and Applications Version 2 (MERRA-2) aerosol reanalysis (Global Modeling and Assimilation Office, 2015), which is used to estimate the relative importance of lead and blowing-snow sea salt emissions compared to transport from the lower latitudes (i.e., northward transport through the high Arctic contour in Fig. 2). Emissions of sea salt in MERRA-2 are computed online at hourly resolution (Randles et al., 2017). Although no validation of MERRA-2 sea salt aerosol is carried out in this work, previous studies on polar aerosols have relied on MERRA-2 data and showed reasonable performance of this product at high latitudes (Xian et al., 2022; Zamora et al., 2022; Böö et al., 2023). However, Lapere et al. (2023) found a large positive bias in sea salt aerosol surface concentrations in MERRA-2 compared to Arctic stations. Therefore, the sea salt aerosol transport computed here is probably an overestimation. Observations of Na^+ atmospheric concentrations at Arctic stations are taken from Norwegian Institute for Air Research (2024) and Yang et al. (2019), and planetary boundary layer heights are taken from Esau and Sorokina (2011). The results presented in this work are all for the year 2018.

3 Results and discussion

3.1 Sensitivity to the choice of sea ice information

In order to evaluate how critical the surface information is for estimating sea spray from leads, we compute emissions in the conceptual model using the three sea ice data sets described in Sect. 2.2 and present them in Figs. 2 and 3. Throughout this section, the fluxes presented are the average of the three source functions (GO03, SA15, IO23) in order to isolate the impact of the choice of the sea ice data set when all other things remain equal. Comparisons between the source functions are presented from Sect. 3.2 onwards.

Using ArcLeads results in lead fractions and emission fluxes more than an order of magnitude larger than with TOPAZ and neXtSIM. This discrepancy can be explained by the detection method in ArcLeads, which is based on thermal contrast from MODIS ice surface temperature data (Reiser et al., 2020). First, the contrast is not strong enough in summer months, which leads to an absence of detection data between May and October. Second, leads covered with a thin layer of ice still have a contrast that is strong enough for them to be detected, whereas we only want to consider the open-water leads for sea spray emissions in the model. In this regard, the ArcLeads product does not provide the fraction of open-water leads at a given moment but rather the fraction of both currently open leads and leads that opened in the previous days that are now covered by thin ice, as the freezing and opening of leads are processes that are faster than the timescale of the satellite observations. This is different from what we extrapolate using the sea ice fraction from TOPAZ/neXtSIM, which is the daily average fraction of open water in the pack ice. This explains why the lead fraction from ArcLeads is so much larger than the lead fractions we derive from TOPAZ and neXtSIM. Leads by definition can be covered by thin ice (WMO, 2014), and this is what Ar-

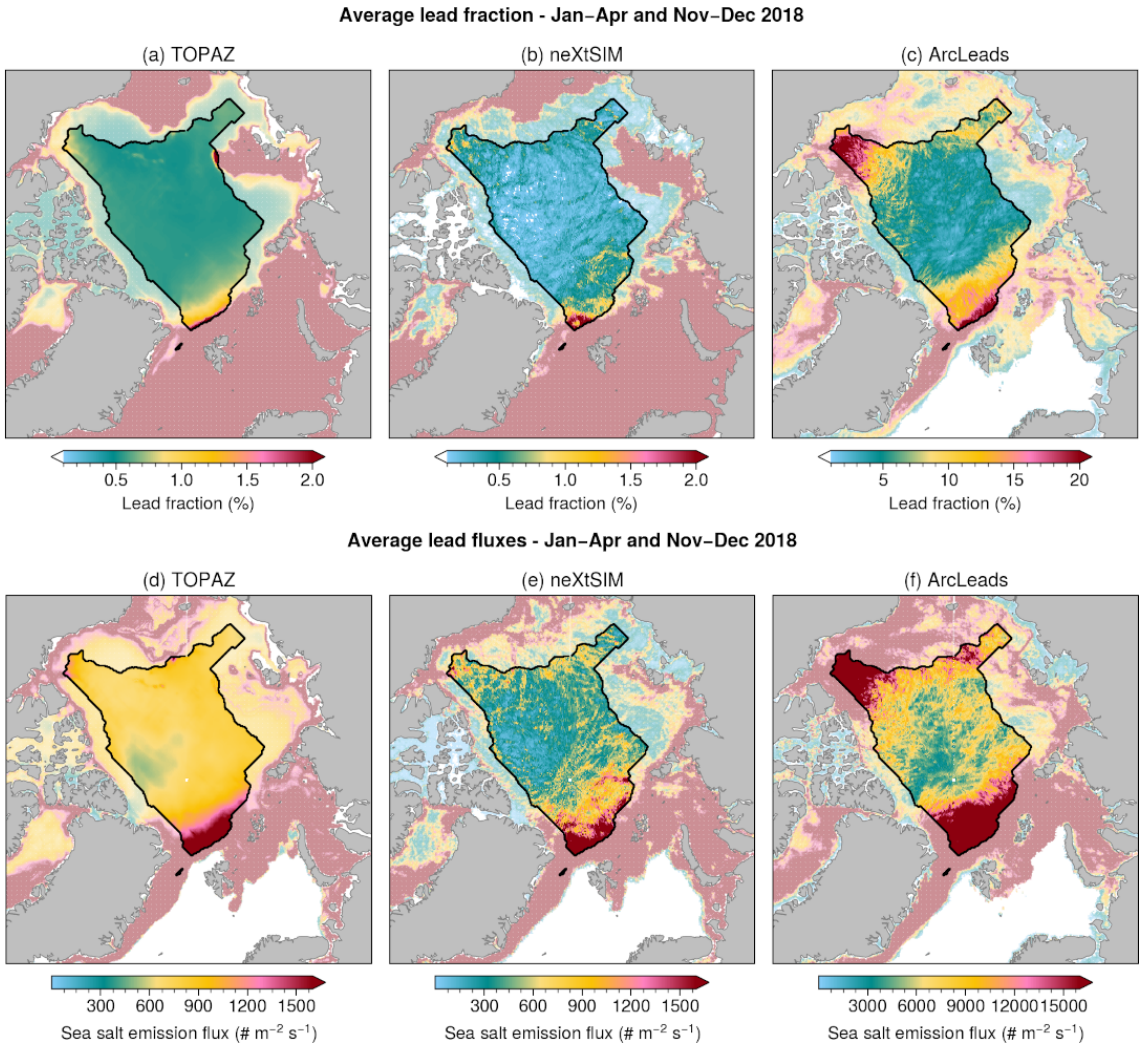

Figure 2. Winter–spring lead fractions and sea salt emissions. Average lead fraction in **(a)** TOPAZ, **(b)** neXtSIM and **(c)** ArcLeads for January–April and November–December 2018. The black contour indicates the area referred to as the high Arctic in this work. Values outside the high Arctic contour are provided for information but are not considered fluxes from leads. Average sea salt particle number emission flux from leads for January–April and November–December 2018 using the average of the three source functions applied to TOPAZ**(d)**, neXtSIM **(e)** and ArcLeads **(f)**. Note that the color scale is different in panel **(c)** and panel **(f)** compared to panels **(a)** and **(b)** and panels **(d)** and **(e)**, respectively.

cLeads provides. But for our study we only need open-water leads. This means that using ArcLeads provides an overestimation of the upper bound of sea spray fluxes from open leads, probably by an order of magnitude, and thus ArcLeads is not usable as is for our sea spray aerosol parameterization. Lead fraction can vary by an order of magnitude in observational lead products depending on the considered physical lead properties, as reported by von Albedyll et al. (2024). There are satellite products that can provide open-water fraction based on ice divergence (e.g., von Albedyll et al., 2024), but they are currently not available on the spatio-temporal scales needed for our study.

Generally, the same spatial distribution of areas of higher sea spray emissions from leads (calculated using the average of the three source functions) appear with the three products for the winter and spring months, as shown in Fig. 2, except in the Beaufort Sea where ArcLeads yields a maximum of lead fraction (around 20 % on average; see Fig. 2c) and therefore an emission hot spot that is not present with the other two products (Fig. 2d–f). The greater lead fractions detected in the Beaufort Sea are discussed in Willmes et al. (2023b) and attributed to stronger wind divergence and thinner sea ice in this area, which leads to more frequent breakup events in winter (Rheinlænder et al., 2024). Both ArcLeads and neXtSIM display patterns typical of leads, showing narrow elongated shapes of increased fluxes, as opposed to the TOPAZ reanalysis, which displays a more homogeneous field without discernible lead shapes. In this regard, neXtSIM

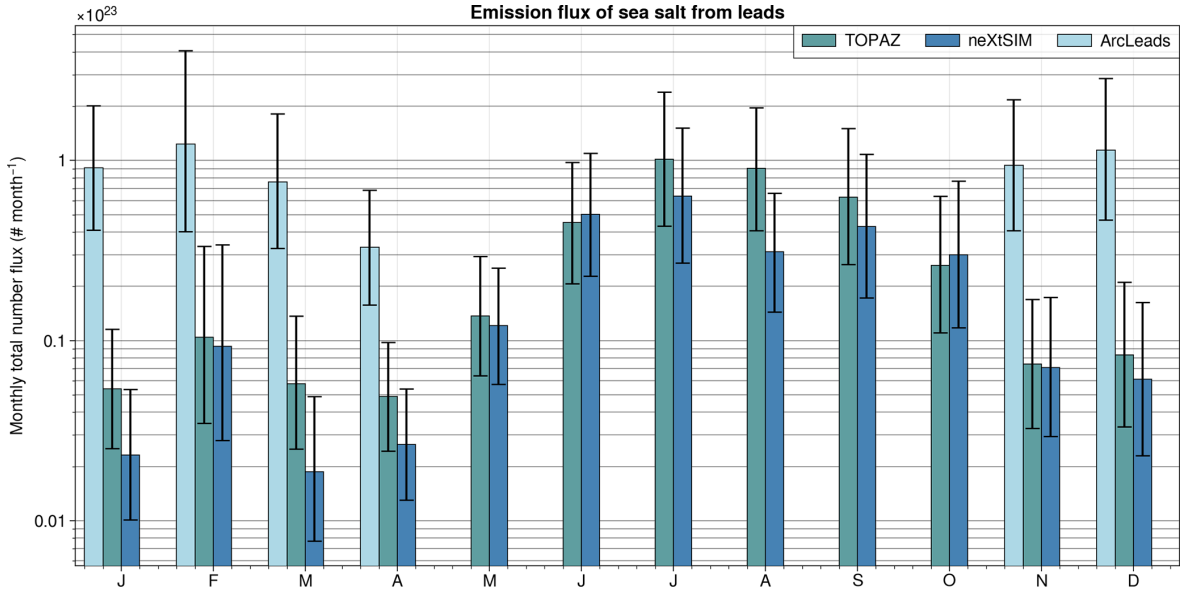

Figure 3. Annual cycle of sea spray emissions from leads. Monthly sum of sea salt aerosol number emissions from leads over the high Arctic using sea ice information from the satellite detection from ArcLeads (light blue), TOPAZ sea ice reanalysis (cadet blue) and sea ice modeling from neXtSIM (steel blue). Error bars indicate the particle number flux obtained using $R_{\mathrm{Nilsson_{min}}}$ and $R_{\mathrm{Nilsson_{max}}}$ instead of R_{Nilsson}. Data for the year 2018 are averaged for the three source functions. Note that the y axis uses a logarithmic scale.

is more appropriate than TOPAZ for detecting leads based on sea ice concentration. Therefore, neXtSIM is the sea ice data set that will be used in the following sections to compute sea spray fluxes from leads.

Major differences in the magnitude of emissions between the three sea ice products are also obtained each month when aggregated at the regional level, as shown in Fig. 3. Similar seasonal cycles and magnitudes are obtained in TOPAZ and neXtSIM, but larger magnitudes are given by ArcLeads. In winter, using ArcLeads generates an emission flux 10 to 15 times larger than with TOPAZ or neXtSIM, albeit with similar variations from month to month (Fig. 3). For this period, TOPAZ and neXtSIM produce similar fluxes, although TOPAZ produces more sea salt aerosol on average. Using both of these model products gives the same seasonality, with maximum emission fluxes between July and September and minimum emissions in March and April that are close to 2 orders of magnitude smaller than in summer. In addition, using $R_{\mathrm{Nilsson_{min}}}$ or $R_{\mathrm{Nilsson_{max}}}$ for the flux computation (error bars in Fig. 3) can result in a difference of up to an order of magnitude in the total particle number flux in the high Arctic.

3.2 Emissions from leads versus blowing snow

Emission of sea salt through blowing snow is known to be an important source of aerosols in sea ice regions (Yang et al., 2008, 2019; Frey et al., 2020; Gong et al., 2023). However, no regional comparison of the relative magnitude of sea salt aerosol fluxes from blowing snow and leads exist at time of writing. In Fig. 4 we compare, for the first time, the seasonal spatial distribution of the sea salt particle number emission flux from blowing snow and leads. In winter, spring and fall, blowing snow in the high Arctic produces sea salt particle number emissions on average 1 to 2 orders of magnitude larger than emissions from leads.

The latter are more heterogeneously distributed and are larger in the area between Greenland, Svalbard and the North Pole. In summer, sea salt number emissions from leads increase and become equivalent to blowing-snow emissions, which are at their annual low, an order of magnitude lower than the other seasons. For that season the spatial distribution of sea spray emissions from leads also differs from the other seasons. Figure 4 also shows that the areas of maximum emission fluxes for blowing snow and leads are not found in the same regions, which is an important characteristic for the pan-Arctic aerosol budget.

The comparison is further studied by aggregating the emissions over the area defined as the high Arctic (see the black contour in Fig. 4). Despite blowing snow dominating the sea salt particle number emissions throughout most of the year (except summer – Figs. 4 and 5a), fluxes from leads in terms of mass emission of sea salt aerosol can be up to 2 orders of magnitude larger than blowing snow, especially in the summer months (Fig. 5b). The difference between number and mass values obtained here is connected to the blowing-snow parameterization releasing mostly fine-mode Na^+ aerosols in large quantities but significantly less coarse-mode aerosol and emissions from leads in our parameterization being much higher for particles bigger than 100 nm (Fig. 1b). Using the IO23 source function results in particle numbers and mass

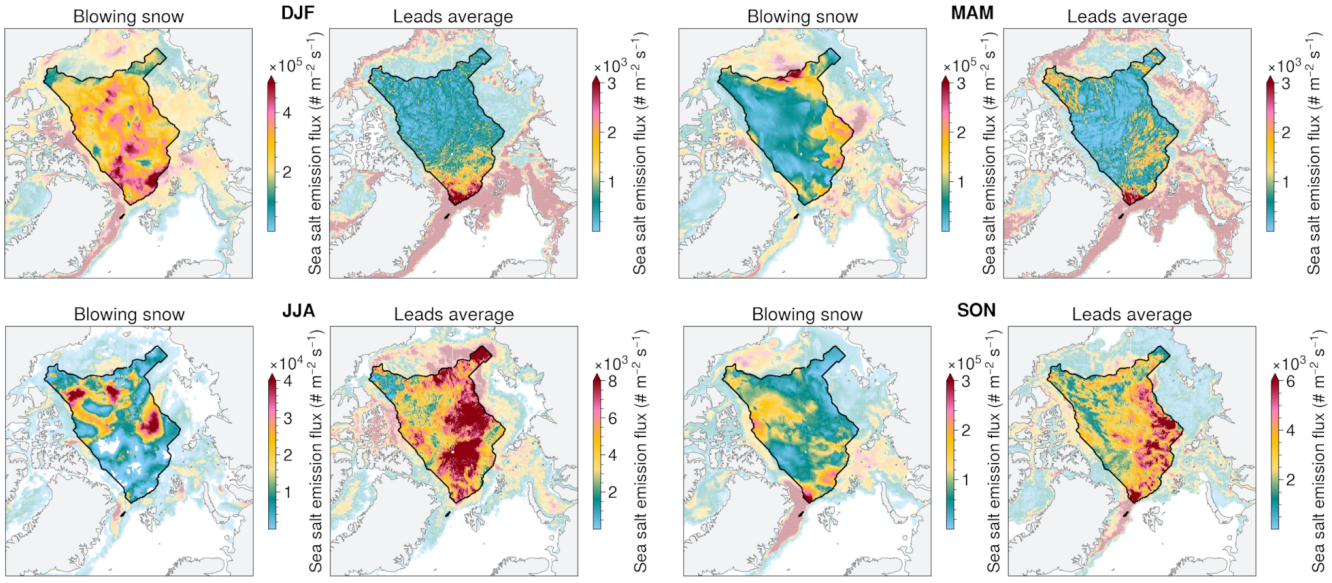

Figure 4. Seasonal emissions from leads and blowing snow. Average particle number emission flux of sea salt aerosol from blowing snow and leads for each season (DJF: December–February; MAM: March–May; JJA: June–August; SON: September–November). The black contour indicates the area defined here as the high Arctic. The average of the three source functions is presented using R_{Nilsson} and neXtSIM sea ice concentration for lead definition. Note that color scales are different from one panel to the other to better show the spatial patterns. Color scales for blowing snow go 1 to 2 orders of magnitude higher than for leads.

fluxes larger than with the GO03 and SA15 source functions, consistent with the size distributions presented in Fig. 1b.

Summed over the whole year, sea salt emissions from leads represent between 0.3 % (with $R_{\mathrm{Nilsson_{min}}}$ and GO03 source function) and 9.8 % (with $R_{\mathrm{Nilsson_{max}}}$ and IO23 source function) of the sea salt number emissions in sea ice regions (i.e., blowing snow plus leads), with mean values (i.e., with R_{Nilsson}) of 0.7 % to 4.5 % depending on the source function. For the sea salt aerosol mass emissions, leads account for a greater fraction, between 30 % and 85 % depending on the parameterization, with mean values of 51 % to 72 %. The greater importance of blowing snow for number emissions and leads for mass emissions is consistent with previous observations, which revealed mostly coarse-size sea salt aerosols from leads (Nilsson et al., 2001; May et al., 2016) and mostly fine-mode sea salt aerosols from blowing snow (Frey et al., 2020; Gong et al., 2023). For cloud-related studies, models using a one-moment cloud microphysics scheme (based on aerosol mass only, e.g., Kessler, 1969) will therefore be more sensitive to emissions from leads, but two-moment schemes (aerosol mass and number, e.g., Morrison et al., 2005) will likely find that sea salt from blowing snow plays a major role.

3.3 Lower and upper bounds of emissions from leads

With the approach and numbers presented above, we can bound the annual mass of sea salt aerosol emitted from leads into the high Arctic atmosphere for the year 2018 between 0.1 and 2.1 Tg yr^{-1} across the three source functions and two sea ice data sets (Fig. 6). For blowing snow, we find a total sea salt aerosol emission flux of 0.2–0.3 Tg yr^{-1} for this region, which is consistent with the results of Confer et al. (2023), who found 0.28–2.24 Tg yr^{-1} for a larger region of the Arctic. In comparison, MERRA-2 gives, for 2018, a mass of sea salt aerosol transported into the high Arctic of 1.8 Tg yr^{-1}. This last number is obtained by integrating the positive component of the meridional total column sea salt aerosol mass flux (SSFLUXV) from MERRA-2 hourly data in 2018 (Global Modeling and Assimilation Office, 2015) along the boundaries of the high Arctic mask shown in Fig. 4. Within these annual totals, the northward transport into the high Arctic is more important in winter months, whereas leads gain importance in the summer months (Fig. 6). Blowing snow shows a similar seasonality to that of transport, albeit with smaller sea salt mass fluxes (around an order of magnitude lower; Fig. 6). Therefore, sea salt emissions from leads and blowing snow may be almost as important as sea salt transported from the open ocean for the aerosol mass budget in the high Arctic.

The uncertainty in sea salt emissions from leads is large, as illustrated by the blue shading in Fig. 6. We evaluate the sensitivity of the sea salt emissions from leads in the high Arctic (both mass and number) to each assumption made in the conceptual model (sea ice data: TOPAZ or neXtSIM; R_{Nilsson} ratio, average, min or max, and source function: GO03, SA15, or IO23). For a given source function and sea ice product, using $R_{\mathrm{Nilsson_{max}}}$ versus $R_{\mathrm{Nilsson_{min}}}$ results in a change in the

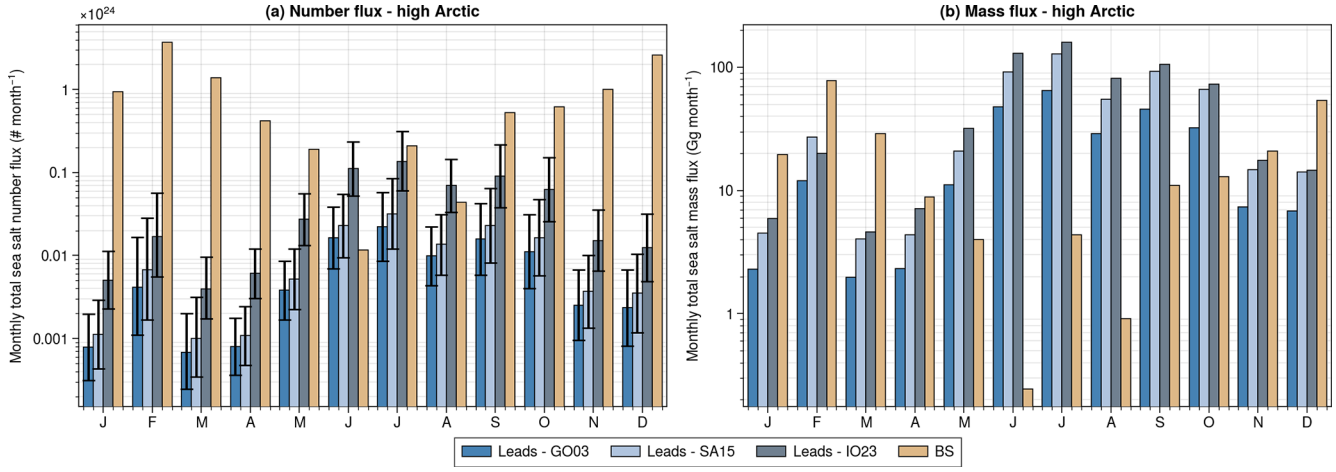

Figure 5. Seasonality of emissions from leads and blowing snow. **(a)** Monthly sum of sea salt particle number emission fluxes integrated over the high Arctic as defined by the black contour in Fig. 4. Steel blue indicates leads using the GO03 source function, light blue indicates leads using the SA15 source function, gray indicates leads using the IO23 source function, and brown indicates blowing snow. Error bars indicate the particle number flux obtained using $R_{\mathrm{Nilsson_{min}}}$ and $R_{\mathrm{Nilsson_{max}}}$ instead of R_{Nilsson}. All values use the neXtSIM sea ice concentration for lead definition. Data are for the year 2018. Panel **(b)** is the same as panel **(a)** but for mass fluxes.

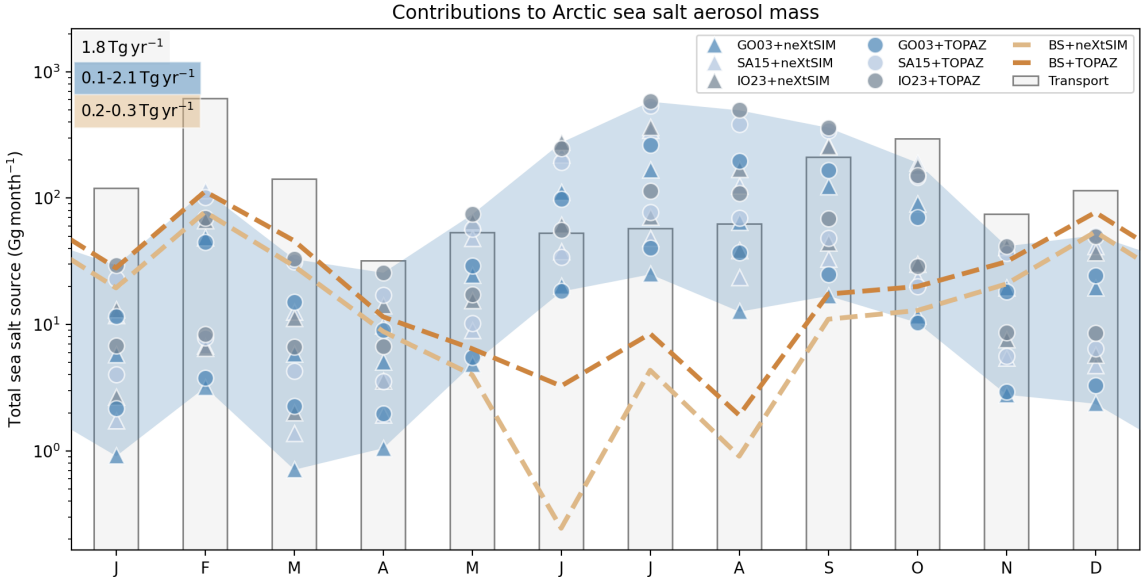

Figure 6. Transport and local production of sea salt aerosol. Monthly total emission and transported sea salt aerosol mass in the high Arctic. Light gray bars show transported sea salt aerosol derived from MERRA-2, blue shading indicates the emission flux from leads using $R_{\mathrm{Nilsson_{min}}}$ (lower bound) and $R_{\mathrm{Nilsson_{max}}}$ (upper bound) for the three source functions and two sea ice data sets, and the dashed brown lines indicate the emission flux from blowing snow using the two sea ice data sets. Annual totals are shown in text boxes. Data are for the year 2018.

total flux of around 132 %–151 %. In comparison, changing the source function for a given R_{Nilsson} and sea ice product results in a 22 %–26 % difference in the total flux between IO23 and SA15 and 85 %–87 % between IO23 and G03. Finally, using TOPAZ versus neXtSIM for a given source function and R_{Nilsson} induces a 35 %–39 % change in the total sea salt aerosol flux.

As explained in Sect. 3.1, emissions from leads computed using ArcLeads are very different from the other two products because ArcLeads includes leads covered by thin ice. The differences between the fluxes obtained with ArcLeads and with the model-based products therefore originate from a different definition of what a lead is rather than uncertainty in the models or the satellite product, and ArcLeads most likely provides an unrealistic upper bound of sea spray fluxes

from leads. Therefore, within our proposed parameterization the largest uncertainty for bounding the sea spray emissions from leads in the Arctic is currently due to the uncertainty and scarcity of emission flux measurements.

3.4 Impact of emissions from leads on the annual cycle of sodium aerosol concentration

Climate models generally do not explicitly consider sea spray emissions from leads or sea salt from blowing snow. Instead, they either ignore sea spray emissions from sea ice regions or apply the open-ocean source function in every grid cell weighted by the open-water fraction. In what follows, this approach is referred to as the "usual approach" and is compared to the approach including sources from leads and blowing snow, with a view to compare the annual cycle of sea salt aerosol obtained with both approaches. In Fig. 7, we show that by replacing the usual approach (dashed black line) with dedicated lead and blowing-snow parameterizations (filled curves) that a better representation of the seasonal cycle of atmospheric concentrations of Na^+ aerosol can be obtained compared to observations (gray bars) at two high-latitude stations affected by sea ice (Alert station, Canada (82.49° N, 62.34° W), and Utqiaġvik station, Alaska (71.2° N, 156.0° W)). Observations at Alert include aerosol sizes up to 1 µm, while Utqiaġvik uses total suspended particles. Here, we remove the condition of being inside the high Arctic mask of Fig. 2 and decide that leads can be found wherever sea ice concentration is greater than 80 %, including in coastal areas near the two stations considered. Although the validity of such an approach needs further investigation, it is necessary here as only coastal stations provide year-long observations with a robust annual cycle. Furthermore, grid points with sea ice concentration below 80 % are ignored since the objective of this part is to assess whether sea ice sources alone can explain the seasonal variations in sea salt aerosols for these locations.

At Alert, the usual approach results in a reversed seasonality compared to observations, with Na^+ aerosol concentrations peaking in summertime, while observations show a wintertime maximum. However, when considering blowing-snow emissions, a wintertime peak in Na^+ aerosol concentration is obtained that is more consistent with observations. Even considering these sea ice sources of sea salt, the seasonality still does not match the observations, which signals that our parameterization could be improved despite already showing better agreement than the usual approach. According to our model, leads at Alert during winter also seem to play a minor role in mass concentrations compared to blowing snow, while during the summer months leads dominate the mass concentration. At Utqiaġvik, observations show maximum Na^+ aerosol concentrations in August–October, consistent with open-ocean-sourced sea salt aerosol, but significant values are also observed in winter months, which the usual approach does not capture (the dashed line is mostly zero outside of September–November). When considering leads and blowing snow, the seasonality in December–July matches very well with the observations. For this location, we find that leads and blowing snow emit similar masses of Na^+ aerosol, although lead emissions are found during a longer period during the year.

Although the method used here to compute the proxy for concentrations has major limitations as it does not account for transport or removal (wet and dry), the annual cycle obtained with the usual approach is similar to the annual cycle of concentrations yielded by climate models from CMIP6 (which use the usual approach for emissions) at these two locations, as shown in Lapere et al. (2023). Therefore, despite the important simplifications in Fig. 7, it strongly suggests that local sea ice sources of sea salt aerosol need to be accounted for to obtain a decent annual cycle of Na^+ concentrations in the coastal Arctic. The absence of sea salt aerosol sources in sea ice regions in climate models was discussed in Lapere et al. (2023) as one reason why CMIP6 models do not compare well with the annual cycle of aerosol observations at high latitudes. With the proxy calculations in Fig. 7 we show that this is indeed likely to explain this current model shortcoming.

3.5 Marine organic fraction of sea spray from leads

Measurements in the high Arctic indicate an important fraction of organic material (OF) in sea spray from leads (Leck et al., 2002; Kirpes et al., 2019), which can affect the ability of sea spray to form liquid droplets (CCN) or ice crystals (INP), as marine aerosols containing organics favor INP conversion over CCN. In what follows, we use the OF parameterization from Vignati et al. (2010) to estimate the OF in sea spray emitted from leads (see Sect. 2) and compare these with observations. The seasonal variations in sea spray OF at the Arctic scale obtained with this parameterization are shown in Fig. 8. Over the open ocean, the OF varies between 20 % in wintertime and a maximum of 45 % in springtime, consistent with the usually observed phytoplankton blooms during that season in the North Atlantic (Cole et al., 2015). In contrast, in sea ice regions the OF is smaller, with a minimum in wintertime of around 17 % and peaks in the fall of 30 % on average. In September, the OF in sea spray from leads is similar to the one in the open ocean. Annually, we estimate that organic material emissions from leads are between 0.02 and 0.35 $Tg\,yr^{-1}$ depending on the choice of source function and $R_{Nilsson}$ ratio. The similar magnitude and complementary seasonality of primary marine organics from the open ocean and from leads is an important characteristic that should be further investigated as it could be critical for cloud nucleation and cloud phase. However, this mass estimate is uncertain because, contrary to the findings from measurement campaigns, we assume the same size distribution at emission for leads and open ocean and for inorganic sea salt and organic material.

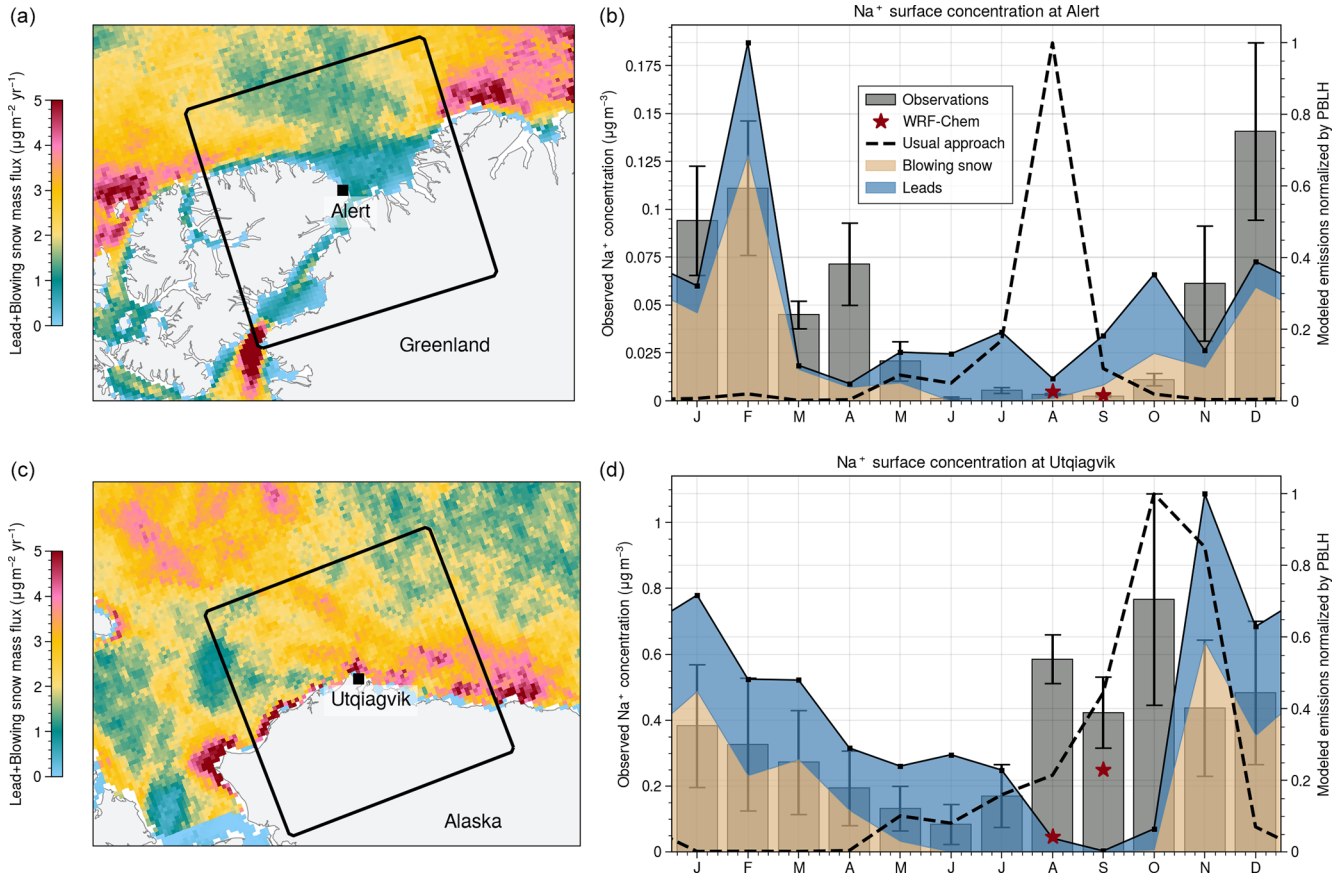

Figure 7. Annual cycle of concentrations at Alert and Utqiaġvik. Annual sea salt aerosol mass flux from blowing snow and leads near the Alert **(a)** and Utqiaġvik **(c)** stations (black square). The black contour indicates the area used for averaging fluxes in the right panel. Monthly mean concentration of Na^+ aerosol at the Alert **(b)** and Utqiaġvik **(d)** stations from observations (Norwegian Institute for Air Research, 2024; Yang et al., 2019; gray bars, with error bars showing 1 standard deviation) and simulated in WRF-Chem (red stars; see Sect. 3.7) and a proxy for concentrations using the open-ocean flux applied to the open-water fraction only (dashed black line) or blowing snow plus leads (filled curves). All time series are normalized by their maximum for readability. For the model, emissions are divided by the boundary layer height values from Esau and Sorokina (2011) to mimic the annual concentration cycle. All fluxes are computed using the mean of the three source functions and average R_{Nilsson}.

The OF values obtained for 2018 in our model are comparable with measurements from past Arctic expeditions. Leck et al. (2002) conducted measurements in the high Arctic during the 1996 Arctic Ocean expedition (AOE-96), including concentrations of sea spray found in the atmosphere near leads. They estimated the OF of the measured sea spray to be 20 % in July–August. Although our data are for the year 2018, we find a consistent OF in sea spray emissions from leads, between 16 %–18 % in July–August (Fig. 9, top row). Similarly, Kirpes et al. (2019) conducted measurements near Utqiaġvik, Alaska, in February 2014 and estimated OF of 30 % to 50 % in sea spray near leads. In our case, for February 2018 we find an OF of 16 % at this location (Fig. 9, bottom row).

One possible explanation for the discrepancy between the OF we model and the measurements by Kirpes et al. (2019) is that their observations may include some transported or aged sea spray and do not solely include freshly emitted aerosols. Figure 8 shows that we predict a higher OF for open-ocean sea spray than for leads during the season of the measurements. Therefore, if the conceptual model considered both leads and transported open-ocean sea spray, we would obtain a higher OF that is closer to the measurements. Furthermore, uncertainties also arise from the chlorophyll *a* product as there are not enough observational data and model biases in both under-ice phytoplankton phenology and sea ice coverage (Wakamatsu et al., 2022). Additionally, massive phytoplankton blooms have been shown to occur under sea ice (Arrigo et al., 2012), which are likely missed by the model since it does not account for light availability under sea ice. Therefore, the use of modeled chlorophyll *a* data has significant uncertainties that are only increased when used for leads.

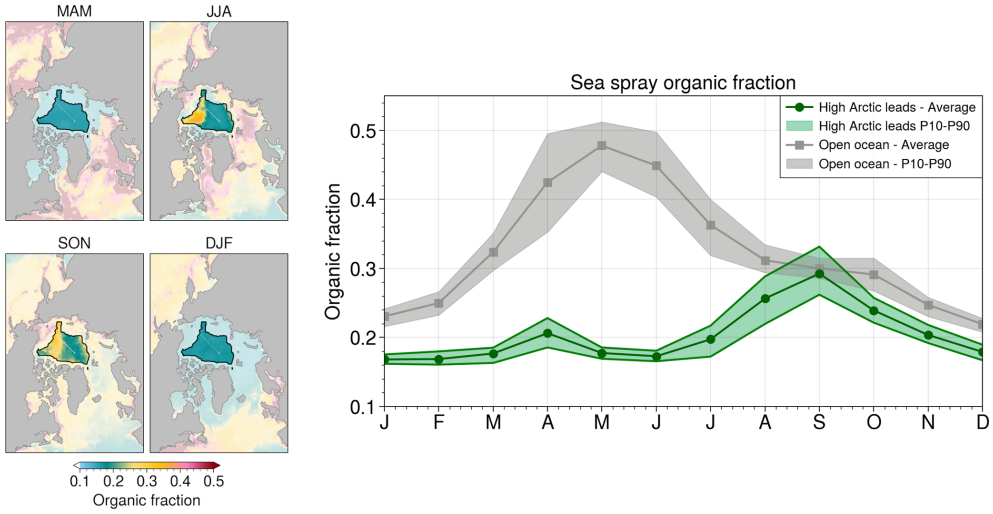

Figure 8. Sea spray organic fraction in the Arctic. Organic fraction in sea spray emissions based on the Vignati et al. (2010) parameterization and Copernicus Marine Service Information (2023b) chlorophyll *a* concentration. The gray line is averaged over the open-ocean areas (i.e., all areas where sea ice concentration is zero within the domain represented in the maps) and weighted by the emission flux. The green line is averaged over lead emission areas in the high Arctic and weighted by the emission flux. The associated shading shows the 10th and 90th percentiles over the corresponding area.

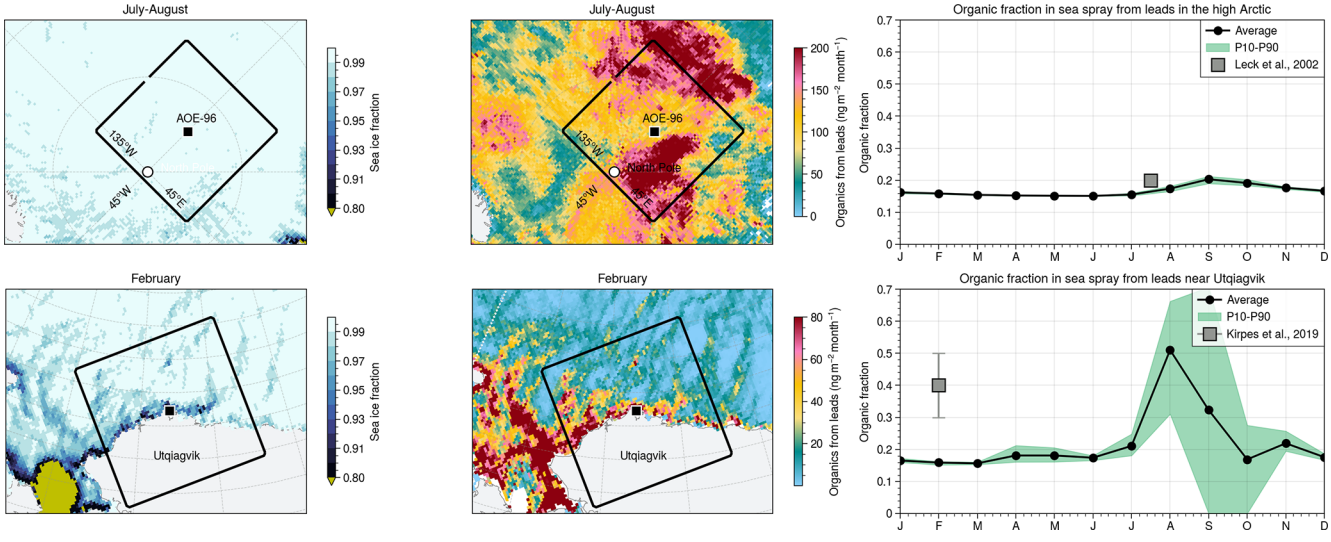

Figure 9. Organic fraction compared to measurements. The top-left panel shows the sea ice fraction in the central Arctic in July–August 2018. The top-middle panel shows the mass flux of organic aerosols from leads in July–August 2018. The black square marks the location where the measurements were made. The top-right panel shows the seasonal cycle of organic mass fraction in sea spray from leads averaged over the black contour in the top-middle panel (black line) and associated 10th and 90th percentiles over the area (green shading). The gray square is the OF measured in July–August 1996 by Leck et al. (2002). The bottom row is the same as top row but for Utqiaġvik station and data from February 2014 by Kirpes et al. (2019).

3.6 Sensitivity of the parameterization

In the process of deriving the parameterization for sea spray emissions from leads proposed in this work, several assumptions are made. Hereafter, we test how sensitive the resulting emissions are to these assumptions.

Following the definition of the marginal ice zone given in Vichi (2022), we define leads as open-water areas within the pack ice when sea ice concentration is above 80 %. Figure A1 shows the monthly sea salt emissions from leads if the threshold on sea ice concentration is taken at 70 % or 90 % instead of 80 %. In the period from November to April, the aggregated emissions in the high Arctic are not sensitive to the threshold choice, since sea ice concentration is higher than 90 % almost everywhere in the domain. The biggest

change is observed in the summer months (June–September), when choosing the more restrictive threshold (90 %) yields an important decrease in emissions, by a factor of 5 in July–August. For that same period, lowering the threshold at 70 % increases the emissions compared to 80 % but less than the decrease obtained with the 90 % threshold. Consistent with the previous results, the sea salt aerosol mass emissions are less sensitive to the threshold than the sea salt aerosol number emissions. Importantly, irrespective of the threshold for leads, blowing snow remains the dominant source in terms of sea salt number emissions throughout the year, and leads remain the dominant sea salt mass emission source in summer months.

For simplicity, only the year 2018 is considered throughout this work for the analysis and evaluation of the parameterization for sea spray emissions from leads. We test the year-to-year variability by computing emissions for the year 2017 as well. Figure A2 shows that the absolute values, seasonal variations, and comparisons between leads and blowing snow are similar for both years. In particular, the total sea salt aerosol mass emission for the high Arctic, using the Gong (2003) source function with R_{Nilsson} ratio, is 0.26 Tg (0.24 Tg, respectively) for leads (blowing snow, respectively) in 2018 and 0.20 Tg (0.26 Tg, respectively) in 2017. This corresponds to a 31 % increase for leads and 6 % decrease for blowing snow between 2017 and 2018. Although the totals are not very different, these variations are still substantial, which indicates that sea spray from leads can account for an important fraction of the inter-annual variability in sea salt mass concentration in the high Arctic.

In Sect. 2.1.3, an assumption is made regarding snow thickness variations to determine whether blowing-snow events can occur. Removing this condition and assuming an infinite snow reservoir instead results in emissions that are around 45 % larger for both sea salt number and mass (Fig. A3) for all periods, with the exception of June. For that month, the emissions increase by an order of magnitude. Although the approach for determining the blowing-snow reservoir adopted in this work needs further refinement, we show that it is not critical for the sea salt aerosol emissions from blowing snow except in summer.

Finally, our work relies on the total aerosol flux measurements by Nilsson et al. (2001). In order to compensate for using only one set of measurements, we explore the whole range of uncertainties from the regressions given by Nilsson et al. (2001), including the confidence interval of the fit coefficients. Importantly, Nilsson et al. (2001) also report measurements of open-ocean total aerosol fluxes (as described by the denominator in Eq. 1). These are similar in magnitude and wind dependence to the total fluxes obtained with the Gong (2003), Salter et al. (2015), and Ioannidis et al. (2023) source function formulations, as shown in Fig. A4. In particular, open-ocean emissions from Nilsson et al. (2001) are very close to Salter et al. (2015). This comparison with usual open-ocean source functions shows that the approach consisting of leveraging measurements from Nilsson et al. (2001) is fit for our purpose.

3.7 Implementation of the lead parameterization in the WRF-Chem model

In order to assess the regional impact of sea spray emissions from leads on aerosol concentrations, the parameterization for sea spray emissions from leads studied throughout this work is also implemented in the 3D regional atmospheric chemistry model WRF-Chem 4.3.3 (code version available at Lapere, 2024). The WRF-Chem model is commonly used for Arctic case studies and generally shows good performance in reproducing atmospheric composition and aerosols in this region, including sea spray (Marelle et al., 2017, 2021; Raut et al., 2022; Ahmed et al., 2023; Ioannidis et al., 2023). A 2-month simulation is conducted for August–September 2018. Summertime is considered because it was identified as the season when sea spray emissions from leads are the highest in Sect. 3.2.

3.7.1 WRF-Chem model setup

A sensitivity analysis, with and without sea spray from leads, is performed for the period 1 August to 30 September 2018, including 17 d of spinup from 15 July to 31 July. The simulation domain at 50 km spatial resolution with 72 vertical levels up to 50 hPa, comprising the Arctic Ocean, is described in Fig. 10.

The sea spray source function used in the WRF-Chem simulations is described in Ioannidis et al. (2023). This source function combines the size distribution from Gong et al. (1997), the wind dependence of the flux from Salisbury et al. (2014), and the SST dependence from Jaeglé et al. (2011). It was shown to be a suitable option for open-ocean Arctic sea spray emissions (Ioannidis et al., 2023). The R_{Nilsson} ratio is then applied on this source function to provide a middle range estimate of the impact of leads on sea spray. The lead fraction is extracted from the neXtSIM product and is taken as the fraction of open water wherever sea ice concentration is greater than 80 %. Sea ice concentration is also taken from neXtSIM in all simulations.

Sea spray emissions in WRF-Chem consist of sodium, chloride, sulfate and organics. The sulfate fraction is computed based on the measurements from Calhoun et al. (1991), and the Vignati et al. (2010) organic fraction is used for primary marine organic emissions (which are attributed to the organic carbon (OC) WRF-Chem species in this model version). Blowing-snow emissions of sea salt aerosol are also activated, following the implementation from Marelle et al. (2021). The aerosol scheme is the Model for Simulating Aerosol Interactions and Chemistry (MOSAIC) with four bins (Zaveri et al., 2008), and the initial and boundary conditions for atmospheric composition are taken from the Community Earth System Model 2.2 with the Community

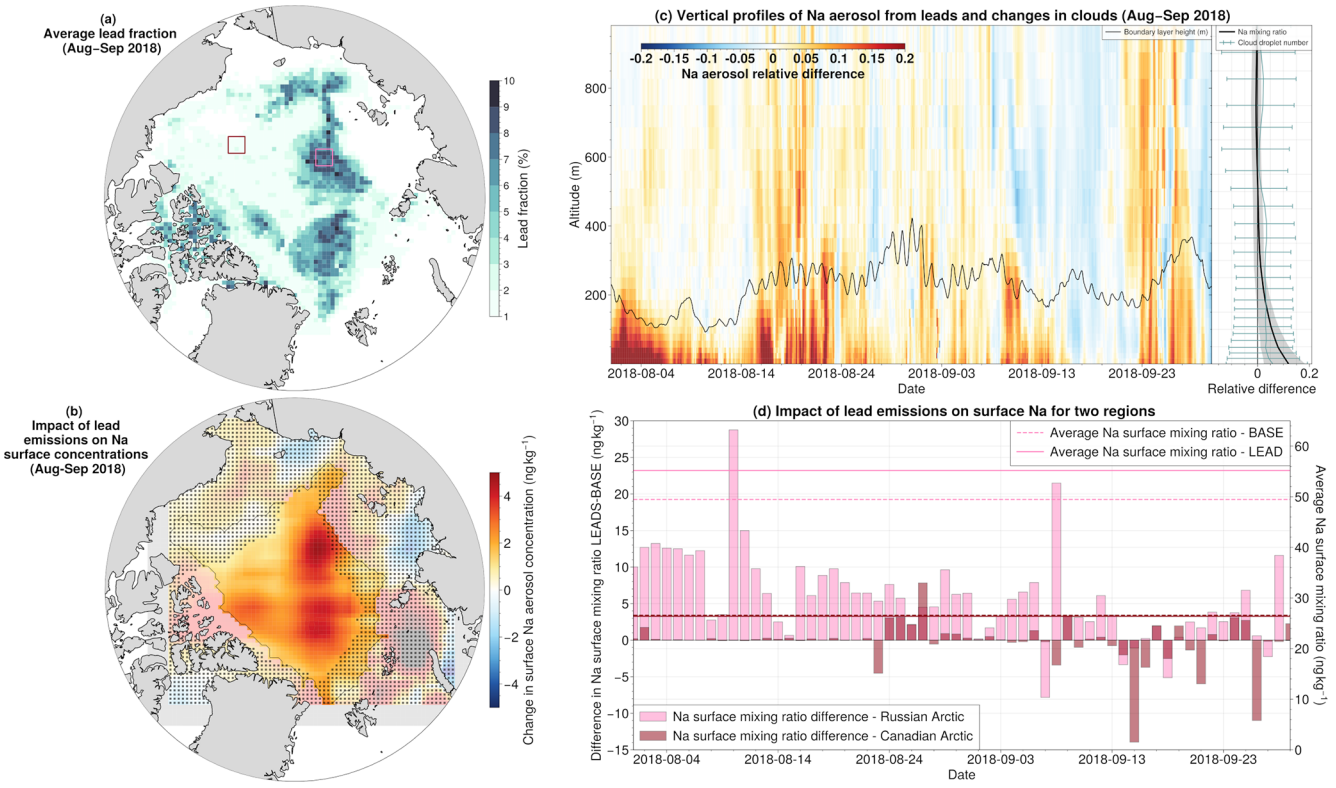

Figure 10. Impact of sea spray emissions from leads in WRF-Chem. **(a)** Average lead fraction over the simulation period extracted from neXtSIM. **(b)** Difference in surface Na mixing ratio between the LEADS and BASE runs. Average over August–September 2018. Stippling indicates grid cells where the change is less than 5 % of the BASE run mixing ratio. The gray band indicates the boundaries of the simulation domain. **(c)** Vertical profiles of relative change between LEADS and BASE averaged over the high Arctic mask in panel **(b)**. On the left is the time evolution of the Na mixing ratio vertical profile, while the right shows the average over the time period for Na (black) and cloud droplet number concentration (blue). Solid lines indicate the mean, while the error bars and shading indicate the 25th and 75th percentiles, respectively. **(d)** Change in daily Na surface mixing ratio in a Canadian Arctic region (red box in panel **(a)** and dark red lines and bars) and in a Russian Arctic region (pink box in panel **(a)** and pink lines and bars). Bars indicate the difference between LEADS and BASE, while lines indicate the average mixing ratio over the period in each simulation.

Atmosphere Model with Chemistry (CESM2.2 CAM-Chem) (Tilmes et al., 2022). Further details of the modeling setup, including boundary and initial conditions and selected parameterizations for meteorology and chemistry, can be found in Table A1.

In order to derive the contribution of leads to sea spray aerosols, two simulations are conducted. A first simulation, referred to as BASE, is conducted with no sea spray emissions from the marginal ice zone or pack ice, meaning that sea spray is disabled as soon as the sea ice concentration is greater than 15 %, which is consistent with the definition of the marginal ice zone given in Vichi (2022). The second simulation activates the lead parameterization described in Sect. 2.1.1, applied where lead fractions are strictly positive, i.e., where sea ice concentration is greater than 80 %. This case is referred to as LEADS. In order to isolate the contribution from leads, in both cases no sea spray is considered in the marginal ice zone, which is between 15 % and 80 % sea ice concentration, and open ocean is considered to be where sea ice concentration is below 15 %. The difference between LEADS and BASE yields an estimate of the aerosol concentrations attributable to sea spray emissions from leads.

The WRF-Chem simulations are evaluated against measurements (Na^+, Cl^- and OC aerosols) from the Zeppelin observatory (Ny-Ålesund, Svalbard) accessed from EBAS (Norwegian Institute for Air Research, 2024). This evaluation is presented in Fig. A5 and shows a good performance of the model for all three species considered. Figure 7 also shows that the magnitude of the monthly averaged Na^+ concentration from the WRF-Chem simulations compares well with observations at Alert and Utqiaġvik.

3.7.2 Impact of leads on sea salt aerosol in WRF-Chem

The location of leads in WRF-Chem as extracted from neXtSIM is shown in Fig. 10a. For the simulation period, leads are mostly found near the North Pole and in the Russian sector of the high Arctic. The lead fractions of up to

10 % on average induce a change between the LEADS and BASE simulations in Na aerosol surface mass mixing ratio (Fig. 10b) by $+2\,\mathrm{ng\,kg^{-1}}$ on average in the high Arctic (black contour in Fig. 10b). Locally, this change can be as high as $+22\,\mathrm{ng\,kg^{-1}}$. These absolute changes correspond to relative changes of 12 % on average and up to more than 30 % of the Na aerosol surface mass mixing ratio in the areas of high lead fraction in the high Arctic (Fig. A6a). For grid points where lead fractions are more than 5 % on average, sea salt emissions from leads account for an average increase in the Na aerosol surface mass mixing ratio of $+3\,\mathrm{ng\,kg^{-1}}$, corresponding to 18 %. Therefore, sea salt emitted from leads accounts for a significant fraction of surface Na aerosol in the Arctic.

The Na aerosol mass mixing ratio is affected by emissions from leads both at the surface and throughout the mixing layer, with the impact decreasing with altitude down to around 2 % near the top of the planetary boundary layer (PBL) in the high Arctic on average (Fig. 10c). These changes include regional differences, as illustrated in Fig. 10d. The Canadian Arctic has very low lead fraction during the simulation period (red box in Fig. 10a), which results in small changes in Na mixing ratio over the period (less than 1 % on the average mixing ratio), although there can be some important changes from day to day (up to 35 %) due to the perturbation of the system induced by the additional emissions at the scale of the simulation domain. In the Russian Arctic, where lead fractions are higher (pink box in Fig. 10a), the average Na surface mixing ratio increases by 12 % in the LEADS case, with daily changes up to 49 %. Therefore, sea salt from leads affects the Arctic in a heterogeneous manner and can account for some of the spatial variability in atmospheric sea salt in the Arctic.

Because of the coupling between the meteorology and the atmospheric composition in WRF-Chem, numerical noise in the sensitivity analysis arises from changes in wind speed and boundary layer height over open-ocean areas (Fig. A6b and c), which results in changes in Na mixing ratio even over open-sea areas. However, these changes outside the sea ice region are smaller than 5 %, as indicated by the stippling in Figs. 10b and A6a, whereas changes due to sea salt emissions from leads contribute more than 5 % over the pack ice.

The changes in cloud cover are also noisy due to the perturbation induced by the changes in Na mixing ratio. Although the average change in cloud droplet number is positive throughout the high Arctic for all vertical levels (around a 3 % increase compared to the BASE simulation) and despite the distribution being skewed towards positive values, the 25th percentile is on average negative (error bars in the rightmost part of Fig. 10c), and the confidence interval at the 95 % level of the mean difference according to a t test contains zero for all vertical levels. Furthermore, although marine organic emissions are included in this version of WRF-Chem, following the methodology described in Sect. 2.1.2, their role as INP has yet to be parameterized. Therefore, as of this version of WRF-Chem, the impact of marine organics from leads on ice clouds is not studied.

4 Conclusions

Based on aerosol fluxes measured in the high Arctic by Nilsson et al. (2001) and sea ice products from numerical models and satellite detection, we propose a parameterization for sea spray emissions from leads in the Arctic Ocean. Using this parameterization under different assumptions (sea ice data, source function, confidence interval of the measurements), we derive upper and lower bounds for the contribution of leads to sea salt aerosol in the high Arctic and investigate its seasonality. Leads contribute between 0.3 % and 9.8 % of the annual sea salt particle number flux emitted locally in the pack ice (i.e., leads plus blowing snow) but 30 % to 85 % of the sea salt aerosol mass flux. The asymmetry between number and mass is connected to the parameterizations of size distributions used in this work, which for both blowing snow and leads are still relatively uncertain and need further observational data. The total annual emitted mass, up to $2.1\,\mathrm{Tg\,yr^{-1}}$, is of the same magnitude as the mass of sea salt transported from the open ocean into the high Arctic in reanalysis data, revealing the critical importance of leads for the aerosol budget in the Arctic. The seasonality of sea spray from leads is found to be anti-phased with blowing snow, with maximum fluxes in summertime, while blowing-snow sea salt aerosol is generated in larger quantities in the winter. We conclude that sea-ice-sourced sea salt aerosols are needed in models to reproduce observed seasonal variations at high latitude.

Furthermore, based on the Vignati et al. (2010) parameterization for sea spray OF, we show that is it possible to reasonably model the organic content of lead-generated sea spray using oceanic chlorophyll a concentration from reanalysis data. Our results agree decently with observed organic fractions of 20 %–50 % in the high Arctic and show greater organic fraction in the fall, as opposed to the open ocean where the organic fraction peaks in the spring. This point is critical for modeling clouds, including cloud phase in the Arctic, and further highlights the importance of modeling sea spray from leads.

The parameterization developed in this work is also implemented in the WRF-Chem model, and a sensitivity test is conducted for 2 months in summertime. The simulations show that including sea spray from leads increases the sea salt mass mixing ratio by around 12 % in the high Arctic for August–September 2018 with regional differences. The important emission fluxes and contributions to concentrations found in this work and the significant organic fraction in sea spray from leads suggest that sea spray from leads could have important impacts on clouds that have yet to be better estimated.

Currently, the largest uncertainty for constraining the sea spray emission flux from leads comes from the confidence interval of the observations used to build the parameterization. In particular, both the magnitude and the sign of the variation in emissions from leads with wind speed are not clearly established depending on the chosen R_{Nilsson}, as illustrated in Fig. 1a, showing increasing $R_{\mathrm{Nilsson_{max}}}$ but decreasing $R_{\mathrm{Nilsson_{min}}}$ as a function of wind speed. This result should motivate future measurement campaigns with designs such that the observed data can readily inform models. In parallel, modeling experiments using the parameterization proposed in this work should be conducted on longer timescales to further estimate the impact of leads on the seasonality of aerosol populations throughout the Arctic atmosphere, including their role in the Arctic climate. Furthermore, because of the choice of lead detection product and because we ignored emissions from the MIZ throughout this work, the estimates of sea spray fluxes presented here are likely lower bounds, which further illustrates the importance of leads for the Arctic aerosol budget. Additionally, although it was developed from an Arctic perspective, this parameterization could be tested for lead emissions in Antarctic sea ice as a first estimate.

Finally, the parameterization proposed in this work can be leveraged to study the relative importance of open-ocean and transported sea spray particles versus particles from open-water areas in sea ice regions in the context of changes in sea ice and the extent of the MIZ. However, as highlighted here, better understandings of aerosol sources in the MIZ and associated parameterizations required to better comprehend Arctic aerosols are still missing.

Appendix A: Appendix

A1 Formulations of sea spray source functions

The Gong (2003) source function describes the wind-dependent sea spray number flux density following Eq. (A1):

$$\begin{aligned}\frac{\mathrm{d}F}{\mathrm{d}r} =& 1.373u^{3.41}r^{-4.7(1+30r)^{-0.017r^{-1.44}}}(1+0.057r^{3.45}) \\ &\times 10^{1.607\exp(-((0.433-\log r)/0.433)^2)},\end{aligned} \tag{A1}$$

where u is the 10 m wind speed and r is the particle radius.

The Salter et al. (2015) source function, which includes a dependency on SST, expresses the sea spray number flux density based on air entrainment, as described in Eq. (A2), using three log-normal modes defined by six parameters each (D_{0i} is the modal diameter; σ_i is the geometric standard deviation; and A_i, B_i, C_i, and D_i are a set of fitting parameters):

$$\begin{aligned}\frac{\mathrm{d}F}{\mathrm{d}\log D} =& 10^{-8}u^{3.74} \\ &\times \sum_{i=1}^{3}\frac{(A_iT^3+B_iT^2+C_iT+D_i)}{\sqrt{2\pi}\log\sigma_i}, \\ &\times \exp\left(-\frac{(\log D-\log D_{0i})^2}{2\log\sigma_i^2}\right)\end{aligned} \tag{A2}$$

where u is the 10 m wind speed, T is the SST in °C and D the particle diameter.

The Ioannidis et al. (2023) source function combines the Gong et al. (1997) size distribution with the whitecap fraction from Salisbury et al. (2014) and the SST dependence from Jaeglé et al. (2011) and includes a correction for smaller particles based on observations from O'Dowd et al. (1997). Its formulation is described in Eq. (A3):

$$\begin{cases}\mathrm{SST_{fac}} = 0.3+0.1T-0.0076T^2+0.00021T^3 \\ \dfrac{\mathrm{d}F}{\mathrm{d}r} = 4.60e^{-5}u^{2.26}3.6e^{5}r^{-3}(1+0.057r^{1.05}) \\ \qquad\qquad \times 10^{1.607\exp(-((0.380-\log r)/0.650)^2)}\mathrm{SST_{fac}} \\ \frac{\mathrm{d}F}{\mathrm{d}r} = \frac{\mathrm{d}F}{\mathrm{d}r}\exp(-0.5(\log(r/0.1)/\log(1.9))^2) \qquad \text{for } r<0.1\end{cases}, \tag{A3}$$

where u is the 10 m wind speed, T is the SST in °C and r is the particle radius.

A2 Sensitivity of the parameterization

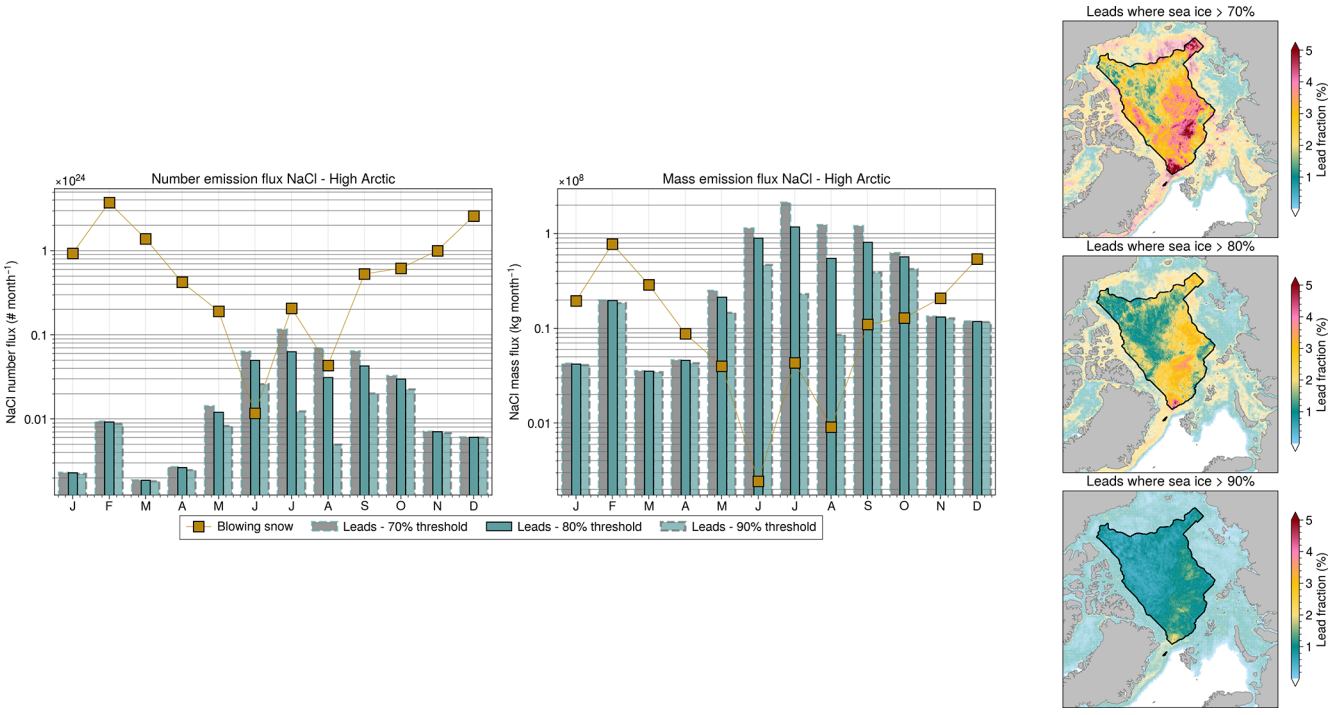

Figure A1. Sensitivity to lead threshold definition. Sea salt aerosol emissions from leads in the high Arctic using an 80 % (darker blue bar, solid line), 70 % (gray bar, dashed line) or 90 % (lighter blue bar, dashed line) sea ice concentration threshold. Brown markers show the particle number flux from blowing snow as a reference. The lead fluxes are the average of the three source functions using the R_{Nilsson} ratio. The sea ice concentration is from neXtSIM. The left panel is the particle number flux, while the middle panel is the particle mass flux. The panels on the right show the annual average lead fraction obtained with each threshold.

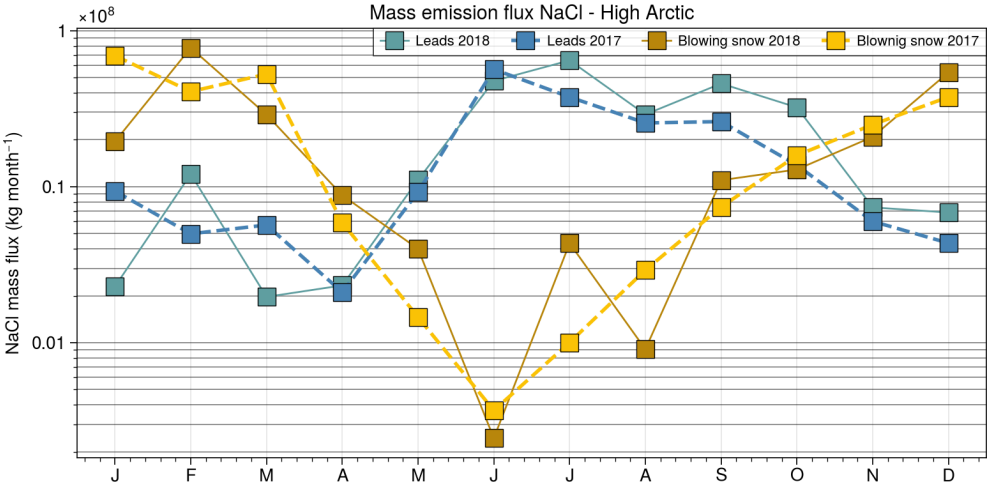

Figure A2. Year-to-year variability. Sea salt aerosol mass flux from blowing snow (yellow) and leads (blue) in the high Arctic for 2018 (darker colors, solid lines) and 2017 (lighter colors, dashed lines). The source function used for lead emissions is Gong (2003) with the R_{Nilsson} ratio. The sea ice concentration is from neXtSIM.

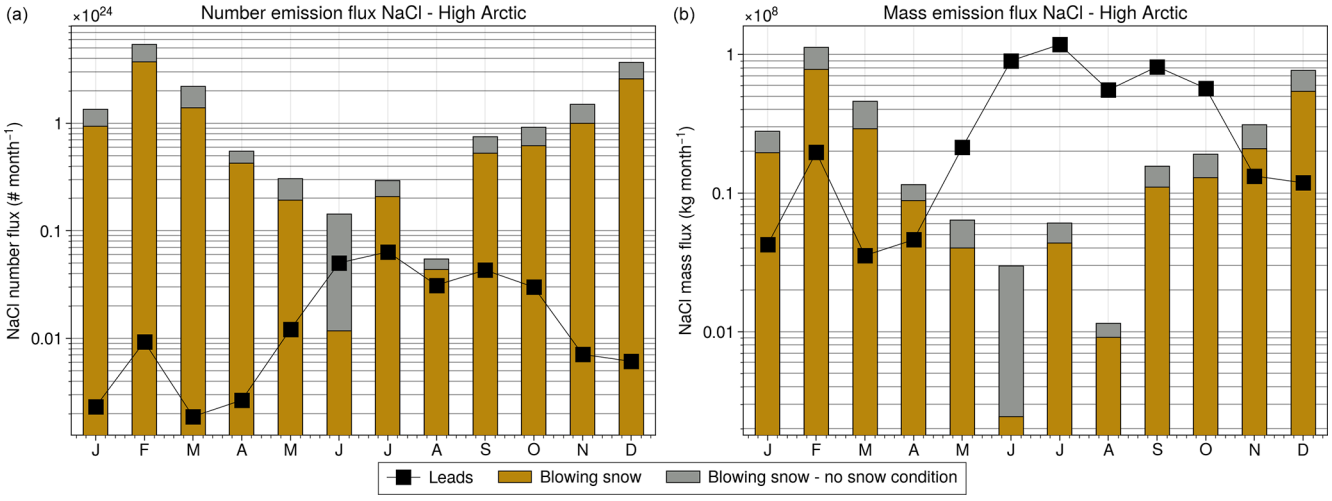

Figure A3. Sensitivity of blowing-snow emissions. Sea salt aerosol emissions from blowing snow in the high Arctic with (brown bar) and without (gray bar) the condition placed on snow thickness variations described in Sect. 2.1.3. Black squares indicate the emissions from leads for reference (average of the three source functions using the R_{Nilsson} ratio). Panel **(a)** is for particle number flux, while panel **(b)** is for particle mass flux.

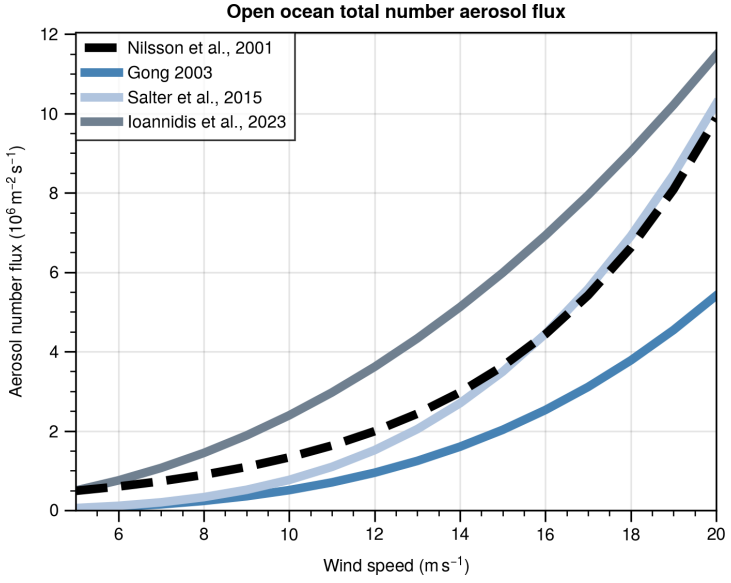

Figure A4. Nilsson et al. (2001) fluxes compared to usual source functions. Total aerosol number flux as a function of wind speed from the Nilsson et al. (2001) measurements (dashed black line – best-fit coefficients) and the Gong (2003) (darker blue line) and Salter et al. (2015) (lighter blue line) source functions. The size distribution used for the source functions is as described in Sect. 2.1.1.

A3 WRF-Chem setup and additional results

Table A1. WRF-Chem model setup.

Physics and meteorology	Model option
Planetary boundary layer / surface layer	MYNN 2.5 level TKE scheme / MYNN (Nakanishi and Niino, 2009)
Surface layer	Noah LSM (Tewari et al., 2004)
Microphysics	Morrison (Morrison et al., 2009)
Shortwave and longwave radiation	RRTMG (Iacono et al., 2008)
Cumulus	Grell-3 (Grell and Dévényi, 2002)
Meteorology IC and BC	NCEP FNL (National Centers for Environmental Prediction et al., 2000)
Aerosol and chemistry	**Model option**
Gas-phase chemistry	MOZART including aqueous-phase chemistry (Emmons et al., 2010)
Aerosols	MOSAIC-4bin (Zaveri et al., 2008)
Chemical IC and BC	CESM2.2: CAM-Chem (Tilmes et al., 2022)
Emissions	**Model option**
Sea spray	Ioannidis (Ioannidis et al., 2023), with organics from Vignati et al. (2010)
Anthropogenic	ECLIPSE v6b (Klimont et al., 2017)
Fire	FINNv1.5 (Wiedinmyer et al., 2014)
Biogenic	MEGAN (Guenther et al., 2012)
DMS	Lana2011 (Lana et al., 2011)

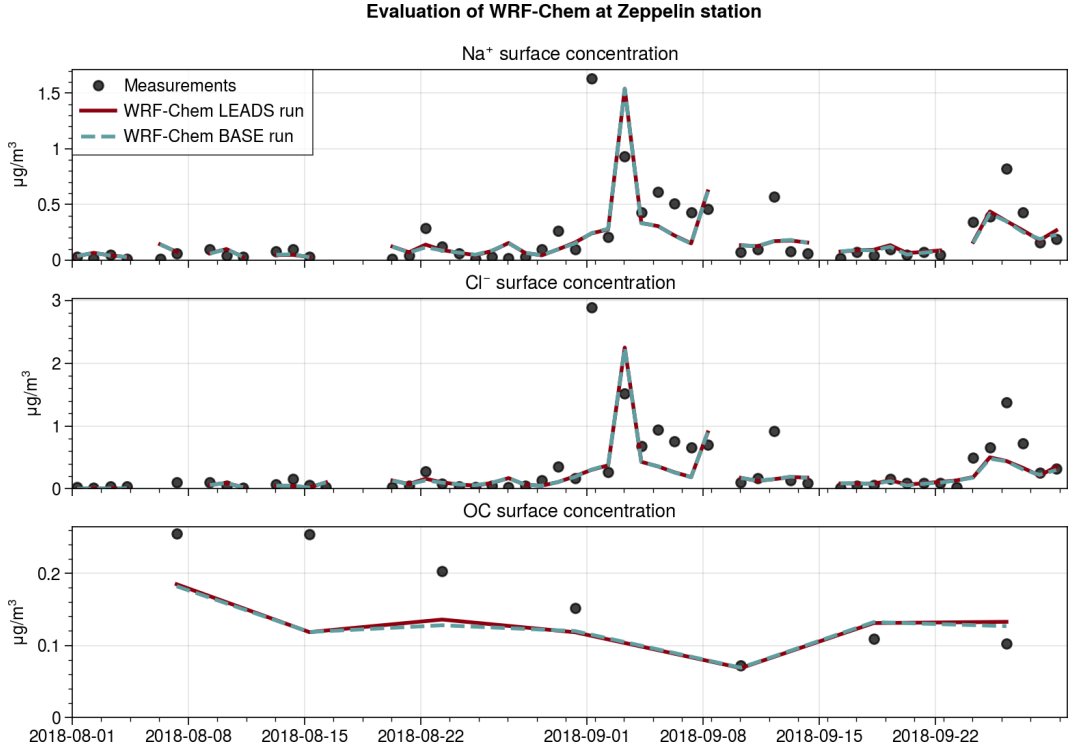

Figure A5. WRF-Chem evaluation. Surface concentration of Na^+, Cl^- and OC at Zeppelin station, Svalbard, in WRF-Chem runs (red is with leads, and blue is without leads) and measured (dots). Observations are total suspended particles.

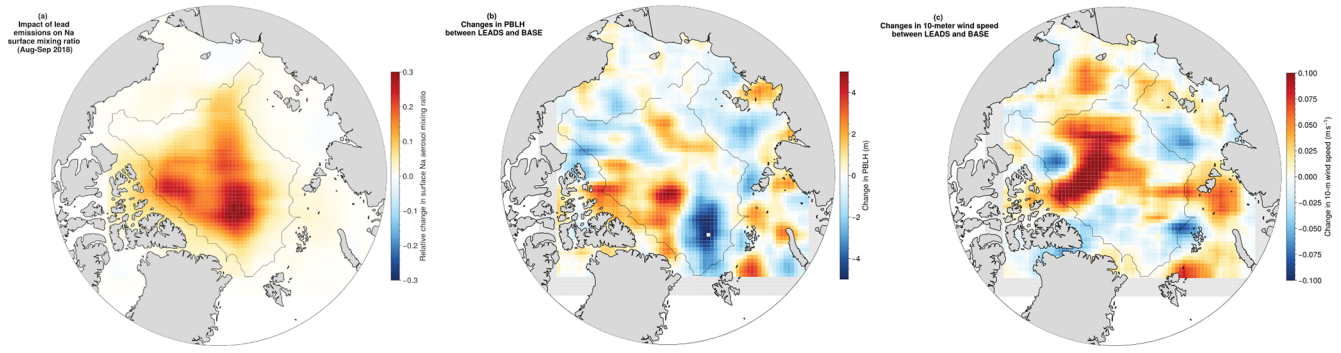

Figure A6. WRF-Chem sensitivity. **(a)** Relative difference in Na surface mixing ratio. **(b)** Difference in PBL height. **(c)** Difference in 10 m hourly maximum wind speed. All panels show average differences between LEADS and BASE simulations for August–September 2018.

Code and data availability. The Python Jupyter Notebooks in which the parameterizations have been implemented are publicly available on Zenodo at https://doi.org/10.5281/zenodo.10782398 (Lapere, 2024). The WRF-Chem model, including our lead emission parameterization, is available at https://doi.org/10.5281/zenodo.10782398 (Lapere, 2024). The neXtSIM sea ice data are available at https://doi.org/10.11582/2024.00114 (Boutin et al., 2024). The satellite lead detection product is available at https://doi.org/10.1594/PANGAEA.955561 (Willmes et al., 2023a). The snow and chlorophyll *a* data are available from https://doi.org/10.48670/moi-00007 (Copernicus Marine Service Information, 2023a) and https://doi.org/10.48670/moi-00019 (Copernicus Marine Service Information, 2023b). Aerosol data from the MERRA-2 reanalysis are available from https://doi.org/10.5067/KLICLTZ8EM9D (Global Modeling and Assimilation Office, 2015). Sodium aerosol measurements at Arctic stations can be found at https://ebas.nilu.no/ (Norwegian Institute for Air Research, 2024). The CAM-Chem boundary conditions used for the WRF-Chem simulations are from https://doi.org/10.5065/XS0R-QE86 (Tilmes et al., 2022), and the meteorological boundary conditions from NCEP FNL can be found at https://doi.org/10.5065/D6M043C6 (National Centers for Environmental Prediction et al., 2000).

Author contributions. Conceptualization: RL, JLT, LM, PR, GS and CM. Formal analysis: RL, JLT and PR. Data curation: RL and LB. Investigation and methodology: RL and JLT. Software: RL and LM. Visualization: RL. Funding acquisition: JLT. Writing – original draft preparation: RL and JLT. Writing – review and editing: LM, PR, LB, GS and CM.

Competing interests. The contact author has declared that none of the authors has any competing interests.

Disclaimer. Publisher's note: Copernicus Publications remains neutral with regard to jurisdictional claims made in the text, published maps, institutional affiliations, or any other geographical representation in this paper. While Copernicus Publications makes every effort to include appropriate place names, the final responsibility lies with the authors.

Acknowledgements. This project has received funding from the European Union's Horizon 2020 research and innovation programme under grant agreement no. 101003826 via the project CRiceS (Climate Relevant interactions and feedbacks: the key role of sea ice and Snow in the polar and global climate system) and under grant agreement no. 101137680 via the project CERTAINTY (Cloud–Aerosol Interactions and Their Impacts in the Earth System). The WRF-Chem simulations were performed using HPC resources from GENCI-IDRIS (grant no. A0150107141). We thank Jean-Christophe Raut, Didier Voisin, and Hélène Angot for the fruitful discussions. Finally, we would like the thank the three reviewers for their valuable insights and comments and the editor for managing this manuscript.

Financial support. This research has been supported by the European Union's Horizon 2020 research and innovation programme under grant agreement no. 101003826 via project CRiceS (Climate Relevant interactions and feedbacks: the key role of sea ice and Snow in the polar and global climate system) and by the Horizon Europe programme under grant agreement no. 101137680 via project CERTAINTY (Cloud-aERosol inTeractions & their impActs IN The earth sYstem).

Review statement. This paper was edited by Johannes Quaas and reviewed by Ruth Price and two anonymous referees.

References

Ahmed, S., Thomas, J. L., Angot, H., Dommergue, A., Archer, S. D., Bariteau, L., Beck, I., Benavent, N., Blechschmidt, A.-M., Blomquist, B., Boyer, M., Christensen, J. H., Dahlke, S., Dastoor, A., Helmig, D., Howard, D., Jacobi, H.-W., Jokinen, T., Lapere, R., Laurila, T., Quéléver, L. L. J., Richter, A., Ryjkov, A., Mahajan, A. S., Marelle, L., Pfaffhuber, K. A., Posman, K., Rinke, A., Saiz-Lopez, A., Schmale, J., Skov, H., Steffen, A., Stupple, G., Stutz, J., Travnikov, O., and Zilker, B.: Modelling the coupled mercury-halogen-ozone cycle in the central Arctic during spring, Elementa: Science of the Anthropocene, 11, 00129, https://doi.org/10.1525/elementa.2022.00129, 2023.

Arrigo, K. R., Perovich, D. K., Pickart, R. S., Brown, Z. W., van Dijken, G. L., Lowry, K. E., Mills, M. M., Palmer, M. A., Balch, W. M., Bahr, F., Bates, N. R., Benitez-Nelson, C., Bowler, B., Brownlee, E., Ehn, J. K., Frey, K. E., Garley, R., Laney, S. R., Lubelczyk, L., Mathis, J., Matsuoka, A., Mitchell, B. G., Moore, G. W. K., Ortega-Retuerta, E., Pal, S., Polashenski, C. M., Reynolds, R. A., Schieber, B., Sosik, H. M., Stephens, M., and Swift, J. H.: Massive Phytoplankton Blooms Under Arctic Sea Ice, Science, 336, 1408–1408, https://doi.org/10.1126/science.1215065, 2012.

Böö, S., Ekman, A. M. L., Svensson, G., and Devasthale, A.: Transport of Mineral Dust Into the Arctic in Two Reanalysis Datasets of Atmospheric Composition, Tellus B, 75, 13–32, https://doi.org/10.16993/tellusb.1866, 2023.

Boutin, G., Ólason, E., Rampal, P., Regan, H., Lique, C., Talandier, C., Brodeau, L., and Ricker, R.: Arctic sea ice mass balance in a new coupled ice–ocean model using a brittle rheology framework, The Cryosphere, 17, 617–638, https://doi.org/10.5194/tc-17-617-2023, 2023.

Boutin, G., Ólason, E., Regan, H., Rampal, P., Brodeau, L., Talandier, C., Lique, C., and Ricker, R.: Data accompanying the article "Arctic sea ice mass balance in a new coupled ice-ocean model using a brittle rheology framework", Norstore [data set], https://doi.org/10.11582/2024.00114, 2024.

Browse, J., Carslaw, K. S., Mann, G. W., Birch, C. E., Arnold, S. R., and Leck, C.: The complex response of Arctic aerosol to sea-ice retreat, Atmos. Chem. Phys., 14, 7543–7557, https://doi.org/10.5194/acp-14-7543-2014, 2014.

Calhoun, J. A., Bates, T. S., and Charlson, R. J.: Sulfur isotope measurements of submicrometer sulfate aerosol particles over the Pacific Ocean, Geophys. Res. Lett., 18, 1877–1880, https://doi.org/10.1029/91GL02304, 1991.

Chen, Q., Mirrielees, J. A., Thanekar, S., Loeb, N. A., Kirpes, R. M., Upchurch, L. M., Barget, A. J., Lata, N. N., Raso, A. R. W., McNamara, S. M., China, S., Quinn, P. K., Ault, A. P., Kennedy, A., Shepson, P. B., Fuentes, J. D., and Pratt, K. A.: Atmospheric particle abundance and sea salt aerosol observations in the springtime Arctic: a focus on blowing snow and leads, Atmos. Chem. Phys., 22, 15263–15285, https://doi.org/10.5194/acp-22-15263-2022, 2022.

Chen, Y., Cheng, Y., Ma, N., Wei, C., Ran, L., Wolke, R., Größ, J., Wang, Q., Pozzer, A., Denier van der Gon, H. A. C., Spindler, G., Lelieveld, J., Tegen, I., Su, H., and Wiedensohler, A.: Natural sea-salt emissions moderate the climate forcing of anthropogenic nitrate, Atmos. Chem. Phys., 20, 771–786, https://doi.org/10.5194/acp-20-771-2020, 2020.

Cole, H. S., Henson, S., Martin, A. P., and Yool, A.: Basin-wide mechanisms for spring bloom initiation: how typical is the North Atlantic?, ICES J. Mar. Sci., 72, 2029–2040, https://doi.org/10.1093/icesjms/fsu239, 2015.

Confer, K. L., Jaeglé, L., Liston, G. E., Sharma, S., Nandan, V., Yackel, J., Ewert, M., and Horowitz, H. M.: Impact of Changing Arctic Sea Ice Extent, Sea Ice Age, and Snow Depth on Sea Salt Aerosol From Blowing Snow and the Open Ocean for 1980–2017, J. Geophys. Res.-Atmos., 128, e2022JD037667, https://doi.org/10.1029/2022JD037667, 2023.

Copernicus Climate Change Service: ERA5: Fifth generation of ECMWF atmospheric reanalyses of the global climate, Copernicus Climate Change Service Climate Data Store (CDS), https://doi.org/10.24381/cds.adbb2d47, 2017.

Copernicus Marine Service Information: Arctic Ocean Physics Reanalysis, Copernicus Marine Service Information (CMEMS), Marine Data Store (MDS) [data set], https://doi.org/10.48670/moi-00007, 2023a.

Copernicus Marine Service Information: Global Ocean Biogeochemistry Hindcast, Copernicus Marine Service Information (CMEMS), Marine Data Store (MDS) [data set], https://doi.org/10.48670/moi-00019, 2023b.

DeMott, P. J., Hill, T. C. J., McCluskey, C. S., Prather, K. A., Collins, D. B., Sullivan, R. C., Ruppel, M. J., Mason, R. H., Irish, V. E., Lee, T., Hwang, C. Y., Rhee, T. S., Snider, J. R., McMeeking, G. R., Dhaniyala, S., Lewis, E. R., Wentzell, J. J. B., Abbatt, J., Lee, C., Sultana, C. M., Ault, A. P., Axson, J. L., Diaz Martinez, M., Venero, I., Santos-Figueroa, G., Stokes, M. D., Deane, G. B., Mayol-Bracero, O. L., Grassian, V. H., Bertram, T. H., Bertram, A. K., Moffett, B. F., and Franc, G. D.: Sea spray aerosol as a unique source of ice nucleating particles, P. Natl. Acad. Sci. USA, 113, 5797–5803, https://doi.org/10.1073/pnas.1514034112, 2016.

Domine, F., Sparapani, R., Ianniello, A., and Beine, H. J.: The origin of sea salt in snow on Arctic sea ice and in coastal regions, Atmos. Chem. Phys., 4, 2259–2271, https://doi.org/10.5194/acp-4-2259-2004, 2004.

Emmons, L. K., Walters, S., Hess, P. G., Lamarque, J.-F., Pfister, G. G., Fillmore, D., Granier, C., Guenther, A., Kinnison, D., Laepple, T., Orlando, J., Tie, X., Tyndall, G., Wiedinmyer, C., Baughcum, S. L., and Kloster, S.: Description and evaluation of the Model for Ozone and Related chemical Tracers, version 4 (MOZART-4), Geosci. Model Dev., 3, 43–67, https://doi.org/10.5194/gmd-3-43-2010, 2010.

Esau, I. and Sorokina, S.: Climatology of the arctic planetary boundary layer, in: Atmospheric Turbulence, Meteorological Modeling and Aerodynamics, edited by: Lang, P. R. and Lombargo, F. S., Nova Science Publishers, Inc., 3–58, ISBN 978-1-60741-091-1, 2011.

Fossum, K. N., Ovadnevaite, J., Ceburnis, D., Dall'Osto, M., Marullo, S., Bellacicco, M., Simó, R., Liu, D., Flynn, M., Zuend, A., and O'Dowd, C.: Summertime Primary and Secondary Contributions to Southern Ocean Cloud Condensation Nuclei, Sci. Rep.-UK, 8, 13844, https://doi.org/10.1038/s41598-018-32047-4, 2018.

Fossum, K. N., Ovadnevaite, J., Ceburnis, D., Preißler, J., Snider, J. R., Huang, R.-J., Zuend, A., and O'Dowd, C.: Sea-spray regulates sulfate cloud droplet activation over oceans, npj Climate and

Atmospheric Science, 3, 1–6, https://doi.org/10.1038/s41612-020-0116-2, 2020.

Frey, M. M., Norris, S. J., Brooks, I. M., Anderson, P. S., Nishimura, K., Yang, X., Jones, A. E., Nerentorp Mastromonaco, M. G., Jones, D. H., and Wolff, E. W.: First direct observation of sea salt aerosol production from blowing snow above sea ice, Atmos. Chem. Phys., 20, 2549–2578, https://doi.org/10.5194/acp-20-2549-2020, 2020.

Fuentes, E., Coe, H., Green, D., de Leeuw, G., and McFiggans, G.: On the impacts of phytoplankton-derived organic matter on the properties of the primary marine aerosol – Part 1: Source fluxes, Atmos. Chem. Phys., 10, 9295–9317, https://doi.org/10.5194/acp-10-9295-2010, 2010.

Gantt, B., Johnson, M. S., Crippa, M., Prévôt, A. S. H., and Meskhidze, N.: Implementing marine organic aerosols into the GEOS-Chem model, Geosci. Model Dev., 8, 619–629, https://doi.org/10.5194/gmd-8-619-2015, 2015.

Gilgen, A., Huang, W. T. K., Ickes, L., Neubauer, D., and Lohmann, U.: How important are future marine and shipping aerosol emissions in a warming Arctic summer and autumn?, Atmos. Chem. Phys., 18, 10521–10555, https://doi.org/10.5194/acp-18-10521-2018, 2018.

Global Modeling and Assimilation Office (GMAO): MERRA-2 tavg1_2d_aer_Nx: 2d,1-Hourly,Time-averaged,Single-Level,Assimilation,Aerosol Diagnostics V5.12.4, Goddard Earth Sciences Data and Information Services Center (GES DISC), Greenbelt, MD, USA [data set], https://doi.org/10.5067/KLICLTZ8EM9D, 2015.

Gong, S. L.: A parameterization of sea-salt aerosol source function for sub- and super-micron particles, Global Biogeochem. Cy., 17, 1097, https://doi.org/10.1029/2003GB002079, 2003.

Gong, S. L., Barrie, L. A., and Blanchet, J.-P.: Modeling sea-salt aerosols in the atmosphere: 1. Model development, J. Geophys. Res.-Atmos., 102, 3805–3818, https://doi.org/10.1029/96JD02953, 1997.

Gong, X., Zhang, J., Croft, B., Yang, X., Frey, M. M., Bergner, N., Chang, R. Y.-W., Creamean, J. M., Kuang, C., Martin, R. V., Ranjithkumar, A., Sedlacek, A. J., Uin, J., Willmes, S., Zawadowicz, M. A., Pierce, J. R., Shupe, M. D., Schmale, J., and Wang, J.: Arctic warming by abundant fine sea salt aerosols from blowing snow, Nat. Geosci., 16, 768–774, https://doi.org/10.1038/s41561-023-01254-8, 2023.

Grell, G. A. and Dévényi, D.: A generalized approach to parameterizing convection combining ensemble and data assimilation techniques, Geophys. Res. Lett., 29, 38-1–38-4, https://doi.org/10.1029/2002GL015311, 2002.

Guenther, A. B., Jiang, X., Heald, C. L., Sakulyanontvittaya, T., Duhl, T., Emmons, L. K., and Wang, X.: The Model of Emissions of Gases and Aerosols from Nature version 2.1 (MEGAN2.1): an extended and updated framework for modeling biogenic emissions, Geosci. Model Dev., 5, 1471–1492, https://doi.org/10.5194/gmd-5-1471-2012, 2012.

Held, A., Brooks, I. M., Leck, C., and Tjernström, M.: On the potential contribution of open lead particle emissions to the central Arctic aerosol concentration, Atmos. Chem. Phys., 11, 3093–3105, https://doi.org/10.5194/acp-11-3093-2011, 2011.

Huang, J. and Jaeglé, L.: Wintertime enhancements of sea salt aerosol in polar regions consistent with a sea ice source from blowing snow, Atmos. Chem. Phys., 17, 3699–3712, https://doi.org/10.5194/acp-17-3699-2017, 2017.

Huang, J., Jaeglé, L., and Shah, V.: Using CALIOP to constrain blowing snow emissions of sea salt aerosols over Arctic and Antarctic sea ice, Atmos. Chem. Phys., 18, 16253–16269, https://doi.org/10.5194/acp-18-16253-2018, 2018.

Iacono, M. J., Delamere, J. S., Mlawer, E. J., Shephard, M. W., Clough, S. A., and Collins, W. D.: Radiative forcing by long-lived greenhouse gases: Calculations with the AER radiative transfer models, J. Geophys. Res.-Atmos., 113, D13103, https://doi.org/10.1029/2008JD009944, 2008.

Ioannidis, E., Law, K. S., Raut, J.-C., Marelle, L., Onishi, T., Kirpes, R. M., Upchurch, L. M., Tuch, T., Wiedensohler, A., Massling, A., Skov, H., Quinn, P. K., and Pratt, K. A.: Modelling wintertime sea-spray aerosols under Arctic haze conditions, Atmos. Chem. Phys., 23, 5641–5678, https://doi.org/10.5194/acp-23-5641-2023, 2023.

Jaeglé, L., Quinn, P. K., Bates, T. S., Alexander, B., and Lin, J.-T.: Global distribution of sea salt aerosols: new constraints from in situ and remote sensing observations, Atmos. Chem. Phys., 11, 3137–3157, https://doi.org/10.5194/acp-11-3137-2011, 2011.

Kessler, E.: On the Distribution and Continuity of Water Substance in Atmospheric Circulations, in: On the Distribution and Continuity of Water Substance in Atmospheric Circulations, American Meteorological Society, ISBN 978-1-935704-36-2, https://doi.org/10.1007/978-1-935704-36-2_1, 1969.

Kirpes, R. M., Bonanno, D., May, N. W., Fraund, M., Barget, A. J., Moffet, R. C., Ault, A. P., and Pratt, K. A.: Wintertime Arctic Sea Spray Aerosol Composition Controlled by Sea Ice Lead Microbiology, ACS Central Science, 5, 1760–1767, https://doi.org/10.1021/acscentsci.9b00541, 2019.

Klimont, Z., Kupiainen, K., Heyes, C., Purohit, P., Cofala, J., Rafaj, P., Borken-Kleefeld, J., and Schöpp, W.: Global anthropogenic emissions of particulate matter including black carbon, Atmos. Chem. Phys., 17, 8681–8723, https://doi.org/10.5194/acp-17-8681-2017, 2017.

Lana, A., Bell, T. G., Simó, R., Vallina, S. M., Ballabrera-Poy, J., Kettle, A. J., Dachs, J., Bopp, L., Saltzman, E. S., Stefels, J., Johnson, J. E., and Liss, P. S.: An updated climatology of surface dimethlysulfide concentrations and emission fluxes in the global ocean, Global Biogeochem. Cy., 25, GB1004, https://doi.org/10.1029/2010GB003850, 2011.

Lapere, R.: Modeling the contribution of leads to sea spray aerosol in the high Arctic, Zenodo [data set and code], https://doi.org/10.5281/zenodo.10782398, 2024.

Lapere, R., Thomas, J. L., Marelle, L., Ekman, A. M. L., Frey, M. M., Lund, M. T., Makkonen, R., Ranjithkumar, A., Salter, M. E., Samset, B. H., Schulz, M., Sogacheva, L., Yang, X., and Zieger, P.: The Representation of Sea Salt Aerosols and Their Role in Polar Climate Within CMIP6, J. Geophys. Res.-Atmos., 128, e2022JD038235, https://doi.org/10.1029/2022JD038235, 2023.

Leck, C., Norman, M., Bigg, E. K., and Hillamo, R.: Chemical composition and sources of the high Arctic aerosol relevant for cloud formation, J. Geophys. Res.-Atmos., 107, 1–17, https://doi.org/10.1029/2001JD001463, 2002.

Li, X., Krueger, S. K., Strong, C., Mace, G. G., and Benson, S.: Midwinter Arctic leads form and dissipate low clouds, Nat. Commun., 11, 206, https://doi.org/10.1038/s41467-019-14074-5, 2020.

Marelle, L., Raut, J.-C., Law, K. S., Berg, L. K., Fast, J. D., Easter, R. C., Shrivastava, M., and Thomas, J. L.: Improvements to the WRF-Chem 3.5.1 model for quasi-hemispheric simulations of aerosols and ozone in the Arctic, Geosci. Model Dev., 10, 3661–3677, https://doi.org/10.5194/gmd-10-3661-2017, 2017.

Marelle, L., Thomas, J. L., Ahmed, S., Tuite, K., Stutz, J., Dommergue, A., Simpson, W. R., Frey, M. M., and Baladima, F.: Implementation and Impacts of Surface and Blowing Snow Sources of Arctic Bromine Activation Within WRF-Chem 4.1.1, J. Adv. Model. Earth Sy., 13, e2020MS002391, https://doi.org/10.1029/2020MS002391, 2021.

May, N. W., Quinn, P. K., McNamara, S. M., and Pratt, K. A.: Multiyear study of the dependence of sea salt aerosol on wind speed and sea ice conditions in the coastal Arctic, J. Geophys. Res.-Atmos., 121, 9208–9219, https://doi.org/10.1002/2016JD025273, 2016.

Monahan, E. C., Spiel, D. E., and Davidson, K. L.: A Model of Marine Aerosol Generation Via Whitecaps and Wave Disruption, in: Oceanic Whitecaps: And Their Role in Air-Sea Exchange Processes, edited by: Monahan, E. C. and Niocaill, G. M., Springer Netherlands, 167–174, https://doi.org/10.1007/978-94-009-4668-2_16, 1986.

Morrison, H., Curry, J. A., and Khvorostyanov, V. I.: A New Double-Moment Microphysics Parameterization for Application in Cloud and Climate Models. Part I: Description, J. Atmos. Sci., 62, 1665–1677, https://doi.org/10.1175/JAS3446.1, 2005.

Morrison, H., Thompson, G., and Tatarskii, V.: Impact of Cloud Microphysics on the Development of Trailing Stratiform Precipitation in a Simulated Squall Line: Comparison of One- and Two-Moment Schemes, Mon. Weather Rev., 137, 991–1007, https://doi.org/10.1175/2008MWR2556.1, 2009.

Nakanishi, M. and Niino, H.: Development of an Improved Turbulence Closure Model for the Atmospheric Boundary Layer, J. Meteorol. Soc. Jpn. Ser. II, 87, 895–912, https://doi.org/10.2151/jmsj.87.895, 2009.

National Centers for Environmental Prediction/National Weather Service/NOAA/U.S. Department of Commerce: NCEP FNL Operational Model Global Tropospheric Analyses, continuing from July 1999, updated daily, Research Data Archive at the National Center for Atmospheric Research, Computational and Information Systems Laboratory [data set], https://doi.org/10.5065/D6M043C6, 2000.

Nilsson, E. D., Rannik, U., Swietlicki, E., Leck, C., Aalto, P. P., Zhou, J., and Norman, M.: Turbulent aerosol fluxes over the Arctic Ocean: 2. Wind-driven sources from the sea, J. Geophys. Res.-Atmos., 106, 32139–32154, https://doi.org/10.1029/2000JD900747, 2001.

Norwegian Institute for Air Research: EBAS [data set], https://ebas.nilu.no/, last access: 1 July 2024.

O'Dowd, C. D., Smith, M. H., Consterdine, I. E., and Lowe, J. A.: Marine aerosol, sea-salt, and the marine sulphur cycle: a short review, Atmos. Environ., 31, 73–80, https://doi.org/10.1016/S1352-2310(96)00106-9, 1997.

Ólason, E., Rampal, P., and Dansereau, V.: On the statistical properties of sea-ice lead fraction and heat fluxes in the Arctic, The Cryosphere, 15, 1053–1064, https://doi.org/10.5194/tc-15-1053-2021, 2021.

Ólason, E., Boutin, G., Korosov, A., Rampal, P., Williams, T., Kimmritz, M., Dansereau, V., and Samaké, A.: A New Brittle Rheology and Numerical Framework for Large-Scale Sea-Ice Models, J. Adv. Model. Earth Sy., 14, e2021MS002685, https://doi.org/10.1029/2021MS002685, 2022.

Prather, K. A., Bertram, T. H., Grassian, V. H., Deane, G. B., Stokes, M. D., DeMott, P. J., Aluwihare, L. I., Palenik, B. P., Azam, F., Seinfeld, J. H., Moffet, R. C., Molina, M. J., Cappa, C. D., Geiger, F. M., Roberts, G. C., Russell, L. M., Ault, A. P., Baltrusaitis, J., Collins, D. B., Corrigan, C. E., Cuadra-Rodriguez, L. A., Ebben, C. J., Forestieri, S. D., Guasco, T. L., Hersey, S. P., Kim, M. J., Lambert, W. F., Modini, R. L., Mui, W., Pedler, B. E., Ruppel, M. J., Ryder, O. S., Schoepp, N. G., Sullivan, R. C., and Zhao, D.: Bringing the ocean into the laboratory to probe the chemical complexity of sea spray aerosol, P. Natl. Acad. Sci. USA, 110, 7550–7555, https://doi.org/10.1073/pnas.1300262110, 2013.

Quinn, P. K., Bates, T. S., Schulz, K. S., Coffman, D. J., Frossard, A. A., Russell, L. M., Keene, W. C., and Kieber, D. J.: Contribution of sea surface carbon pool to organic matter enrichment in sea spray aerosol, Nat. Geosci., 7, 228–232, https://doi.org/10.1038/ngeo2092, 2014.

Quinn, P. K., Coffman, D. J., Johnson, J. E., Upchurch, L. M., and Bates, T. S.: Small fraction of marine cloud condensation nuclei made up of sea spray aerosol, Nat. Geosci., 10, 674–679, https://doi.org/10.1038/ngeo3003, 2017.

Radke, L. F., Hobbs, P. V., and Pinnons, J. E.: Observations of Cloud Condensation Nuclei, Sodium-Containing Particles, Ice Nuclei and the Light-Scattering Coefficient Near Barrow, Alaska, J. Appl. Meteorol. Clim., 15, 982–995, https://doi.org/10.1175/1520-0450(1976)015<0982:OOCCNS>2.0.CO;2, 1976.

Rampal, P., Bouillon, S., Ólason, E., and Morlighem, M.: neXtSIM: a new Lagrangian sea ice model, The Cryosphere, 10, 1055–1073, https://doi.org/10.5194/tc-10-1055-2016, 2016.

Rampal, P., Dansereau, V., Olason, E., Bouillon, S., Williams, T., Korosov, A., and Samaké, A.: On the multi-fractal scaling properties of sea ice deformation, The Cryosphere, 13, 2457–2474, https://doi.org/10.5194/tc-13-2457-2019, 2019.

Randles, C. A., Da Silva, A. M., Buchard, V., Colarco, P. R., Darmenov, A., Govindaraju, R., Smirnov, A., Holben, B., Ferrare, R., Hair, J., Shinozuka, Y., and Flynn, C. J.: The MERRA-2 Aerosol Reanalysis, 1980 – onward, Part I: System Description and Data Assimilation Evaluation, J. Climate, 30, 6823–6850, https://doi.org/10.1175/JCLI-D-16-0609.1, 2017.

Raut, J.-C., Law, K. S., Onishi, T., Daskalakis, N., and Marelle, L.: Impact of shipping emissions on air pollution and pollutant deposition over the Barents Sea, Environ. Pollut., 298, 118832, https://doi.org/10.1016/j.envpol.2022.118832, 2022.

Reiser, F., Willmes, S., and Heinemann, G.: A New Algorithm for Daily Sea Ice Lead Identification in the Arctic and Antarctic Winter from Thermal-Infrared Satellite Imagery, Remote Sens.-Basel, 12, 1957, https://doi.org/10.3390/rs12121957, 2020.

Rheinlænder, J. W., Regan, H., Rampal, P., Boutin, G., Ólason, E., and Davy, R.: Breaking the Ice: Exploring the Changing Dynamics of Winter Breakup Events in the Beaufort Sea, J. Geophys. Res.-Oceans, 129, e2023JC020395, https://doi.org/10.1029/2023JC020395, 2024.

Rinaldi, M., Fuzzi, S., Decesari, S., Marullo, S., Santoleri, R., Provenzale, A., von Hardenberg, J., Ceburnis, D., Vaishya, A., O'Dowd, C. D., and Facchini, M. C.: Is chlorophyll *a* the best

surrogate for organic matter enrichment in submicron primary marine aerosol?, J. Geophys. Res.-Atmos., 118, 4964–4973, https://doi.org/10.1002/jgrd.50417, 2013.

Rocchi, A., von Jackowski, A., Welti, A., Li, G., Kanji, Z. A., Povazhnyy, V., Engel, A., Schmale, J., Nenes, A., Berdalet, E., Simó, R., and Dall'Osto, M.: Glucose Enhances Salinity-Driven Sea Spray Aerosol Production in Eastern Arctic Waters, Environ. Sci. Technol., 58, 8748–8759, https://doi.org/10.1021/acs.est.4c02826, 2024.

Sakov, P., Counillon, F., Bertino, L., Lisæter, K. A., Oke, P. R., and Korablev, A.: TOPAZ4: an ocean-sea ice data assimilation system for the North Atlantic and Arctic, Ocean Sci., 8, 633–656, https://doi.org/10.5194/os-8-633-2012, 2012.

Salisbury, D. J., Anguelova, M. D., and Brooks, I. M.: Global distribution and seasonal dependence of satellite-based whitecap fraction, Geophys. Res. Lett., 41, 1616–1623, https://doi.org/10.1002/2014GL059246, 2014.

Salter, M. E., Zieger, P., Acosta Navarro, J. C., Grythe, H., Kirkevåg, A., Rosati, B., Riipinen, I., and Nilsson, E. D.: An empirically derived inorganic sea spray source function incorporating sea surface temperature, Atmos. Chem. Phys., 15, 11047–11066, https://doi.org/10.5194/acp-15-11047-2015, 2015.

Sand, M., Samset, B. H., Balkanski, Y., Bauer, S., Bellouin, N., Berntsen, T. K., Bian, H., Chin, M., Diehl, T., Easter, R., Ghan, S. J., Iversen, T., Kirkevåg, A., Lamarque, J.-F., Lin, G., Liu, X., Luo, G., Myhre, G., Noije, T. V., Penner, J. E., Schulz, M., Seland, Ø., Skeie, R. B., Stier, P., Takemura, T., Tsigaridis, K., Yu, F., Zhang, K., and Zhang, H.: Aerosols at the poles: an AeroCom Phase II multi-model evaluation, Atmos. Chem. Phys., 17, 12197–12218, https://doi.org/10.5194/acp-17-12197-2017, 2017.

Satheesh, S. K. and Lubin, D.: Short wave versus long wave radiative forcing by Indian Ocean aerosols: Role of sea-surface winds, Geophys. Res. Lett., 30, 1695, https://doi.org/10.1029/2003GL017499, 2003.

Strong, C. and Rigor, I. G.: Arctic marginal ice zone trending wider in summer and narrower in winter, Geophys. Res. Lett., 40, 4864–4868, https://doi.org/10.1002/grl.50928, 2013.

Struthers, H., Ekman, A. M. L., Glantz, P., Iversen, T., Kirkevåg, A., Mårtensson, E. M., Seland, Ø., and Nilsson, E. D.: The effect of sea ice loss on sea salt aerosol concentrations and the radiative balance in the Arctic, Atmos. Chem. Phys., 11, 3459–3477, https://doi.org/10.5194/acp-11-3459-2011, 2011.

Takemura, T., Nakajima, T., Dubovik, O., Holben, B. N., and Kinne, S.: Single-Scattering Albedo and Radiative Forcing of Various Aerosol Species with a Global Three-Dimensional Model, J. Climate, 15, 333–352, https://doi.org/10.1175/1520-0442(2002)015<0333:SSAARF>2.0.CO;2, 2002.

Tewari, M., Chen, F., Wang, W., Dudhia, J., LeMone, M., Gayno, G., Wegiel, J., and Cuenca, R.: Implementation and verification of the unified Noah land surface model in the WRF model, 20th Conference on Weather Analysis and Forecasting/16th Conference on Numerical Weather Prediction, 14 January 2004, Seattle, WA, USA, American Meteorological Society, Seattle, WA, 2004.

Thornhill, G., Collins, W., Olivié, D., Skeie, R. B., Archibald, A., Bauer, S., Checa-Garcia, R., Fiedler, S., Folberth, G., Gjermundsen, A., Horowitz, L., Lamarque, J.-F., Michou, M., Mulcahy, J., Nabat, P., Naik, V., O'Connor, F. M., Paulot, F., Schulz, M., Scott, C. E., Séférian, R., Smith, C., Takemura, T., Tilmes, S., Tsigaridis, K., and Weber, J.: Climate-driven chemistry and aerosol feedbacks in CMIP6 Earth system models, Atmos. Chem. Phys., 21, 1105–1126, https://doi.org/10.5194/acp-21-1105-2021, 2021.

Tilmes, S., Emmons, L., Buchholz, R., and The CESM2 Development Team: CESM2.2 CAM-chem as Boundary Conditions, Research Data Archive at the National Center for Atmospheric Research, Computational and Information Systems Laboratory [data set], https://doi.org/10.5065/XS0R-QE86, 2022.

Vichi, M.: An indicator of sea ice variability for the Antarctic marginal ice zone, The Cryosphere, 16, 4087–4106, https://doi.org/10.5194/tc-16-4087-2022, 2022.

Vignati, E., Facchini, M., Rinaldi, M., Scannell, C., Ceburnis, D., Sciare, J., Kanakidou, M., Myriokefalitakis, S., Dentener, F., and O'Dowd, C.: Global scale emission and distribution of sea-spray aerosol: Sea-salt and organic enrichment, Atmos. Environ., 44, 670–677, https://doi.org/10.1016/j.atmosenv.2009.11.013, 2010.

von Albedyll, L., Hendricks, S., Hutter, N., Murashkin, D., Kaleschke, L., Willmes, S., Thielke, L., Tian-Kunze, X., Spreen, G., and Haas, C.: Lead fractions from SAR-derived sea ice divergence during MOSAiC, The Cryosphere, 18, 1259–1285, https://doi.org/10.5194/tc-18-1259-2024, 2024.

Wakamatsu, T., Yumruktepe, C., Samuelsen, A., and Bertino, L.: QUALITY INFORMATION DOCUMENT For Arctic Biological Reanalysis Product ARCTIC_MULTIYEAR_BGC_002_005, Tech. rep., Copernicus Marine Environment Monitoring Service Information, https://catalogue.marine.copernicus.eu/documents/QUID/CMEMS-ARC-QUID-002-005.pdf (last access: 1 July 2024), 2022.

Wang, X., Deane, G. B., Moore, K. A., Ryder, O. S., Stokes, M. D., Beall, C. M., Collins, D. B., Santander, M. V., Burrows, S. M., Sultana, C. M., and Prather, K. A.: The role of jet and film drops in controlling the mixing state of submicron sea spray aerosol particles, P. Natl. Acad. Sci. USA, 114, 6978–6983, https://doi.org/10.1073/pnas.1702420114, 2017.

Wiedinmyer, C., Yokelson, R. J., and Gullett, B. K.: Global Emissions of Trace Gases, Particulate Matter, and Hazardous Air Pollutants from Open Burning of Domestic Waste, Environ. Sci. Technol., 48, 9523–9530, https://doi.org/10.1021/es502250z, 2014.

Willmes, S., Heinemann, G., and Reiser, F.: ArcLeads: Daily sea-ice lead maps for the Arctic, 2002–2021, NOV–APR, PANGAEA [data set], https://doi.org/10.1594/PANGAEA.955561, 2023a.

Willmes, S., Heinemann, G., and Schnaase, F.: Patterns of wintertime Arctic sea-ice leads and their relation to winds and ocean currents, The Cryosphere, 17, 3291–3308, https://doi.org/10.5194/tc-17-3291-2023, 2023b.

Wilson, T. W., Ladino, L. A., Alpert, P. A., Breckels, M. N., Brooks, I. M., Browse, J., Burrows, S. M., Carslaw, K. S., Huffman, J. A., Judd, C., Kilthau, W. P., Mason, R. H., McFiggans, G., Miller, L. A., Nájera, J. J., Polishchuk, E., Rae, S., Schiller, C. L., Si, M., Temprado, J. V., Whale, T. F., Wong, J. P. S., Wurl, O., Yakobi-Hancock, J. D., Abbatt, J. P. D., Aller, J. Y., Bertram, A. K., Knopf, D. A., and Murray, B. J.: A marine biogenic source of atmospheric ice-nucleating particles, Nature, 525, 234–238, https://doi.org/10.1038/nature14986, 2015.

WMO: Sea Ice Nomenclature, https://library.wmo.int/index.php?lvl=notice_display&id=6772, last access: 1 April 2024.

Xian, P., Zhang, J., O'Neill, N. T., Toth, T. D., Sorenson, B., Colarco, P. R., Kipling, Z., Hyer, E. J., Campbell, J. R., Reid, J. S., and Ranjbar, K.: Arctic spring and summertime aerosol optical depth baseline from long-term observations and model reanalyses – Part 1: Climatology and trend, Atmos. Chem. Phys., 22, 9915–9947, https://doi.org/10.5194/acp-22-9915-2022, 2022.

Xu, L., Russell, L. M., and Burrows, S. M.: Potential sea salt aerosol sources from frost flowers in the pan-Arctic region: Salt Aerosol Sources from Frost Flowers, J. Geophys. Res.-Atmos., 121, 10840–10856, https://doi.org/10.1002/2015JD024713, 2016.

Yang, X., Pyle, J. A., and Cox, R. A.: Sea salt aerosol production and bromine release: Role of snow on sea ice, Geophys. Res. Lett., 35, L16815, https://doi.org/10.1029/2008GL034536, 2008.

Yang, X., Frey, M. M., Rhodes, R. H., Norris, S. J., Brooks, I. M., Anderson, P. S., Nishimura, K., Jones, A. E., and Wolff, E. W.: Sea salt aerosol production via sublimating wind-blown saline snow particles over sea ice: parameterizations and relevant microphysical mechanisms, Atmos. Chem. Phys., 19, 8407–8424, https://doi.org/10.5194/acp-19-8407-2019, 2019.

Zamora, L. M., Kahn, R. A., Evangeliou, N., Groot Zwaaftink, C. D., and Huebert, K. B.: Comparisons between the distributions of dust and combustion aerosols in MERRA-2, FLEXPART, and CALIPSO and implications for deposition freezing over wintertime Siberia, Atmos. Chem. Phys., 22, 12269–12285, https://doi.org/10.5194/acp-22-12269-2022, 2022.

Zaveri, R. A., Easter, R. C., Fast, J. D., and Peters, L. K.: Model for Simulating Aerosol Interactions and Chemistry (MOSAIC), J. Geophys. Res.-Atmos., 113, D13204, https://doi.org/10.1029/2007JD008782, 2008.